Synthesis and Characterization of Copper (II) Sulfide & Cobalt Silicate Composites for Enhanced Cationic Dye Degradation from Aqueous Solution

Yeshitla Tsegaw Gizaw

A Thesis Submitted to
The department of Materials Science and Engineering

School of Mechanical, Chemical, and Materials Engineering

Presented in Partial Fulfillment of the Requirement for the Degree of Master's in Materials Science and Engineering

Office of Graduate Studies
Adama Science and Technology University

August 2021
Adama, Ethiopia

Synthesis and Characterization of Copper (II) Sulfide & Cobalt Silicate Composites for Enhanced Cationic Dye Degradation from Aqueous Solution

Mr. Yeshitla Tsegaw Gizaw

Main Advisor: Dr. Dinsefa Mensur Andoshe

Co- advisor: Dr. Osman Ahmed Zelekew

A Thesis Submitted to
The department of Materials Science and Engineering

School of Mechanical, Chemical, and Materials Engineering,

Presented in Partial Fulfillment of the Requirement for the Degree of Master's in Material Science and Engineering

Office of Graduate Studies
Adama Science and Technology University

August 2021
Adama, Ethiopia

DECLARATION

I hereby declare that this Master Thesis entitled **"Synthesis and Characterization of Copper (II) Sulfide & Cobalt Silicate Composites for Enhanced Cationic Dye Degradation from Aqueous Solution"** is my original work. That is, it has not been submitted for the award of any academic degree, diploma, or certificate in any other university. All sources of materials that are used for this thesis have been duly acknowledged through citation.

_____ _____ _____

Name of the Student Signature Date

RECOMMENDATION

We, the advisors of this thesis, hereby certify that I have read the revised version of the thesis entitled **"Synthesis and Characterization of Copper (II) Sulfide & Cobalt Silicate Composites for Enhanced Cationic Dye Degradation from Aqueous Solution"** prepared under my guidance by Yeshitla Tsegaw Gizaw submitted in partial fulfillment of the requirements for the degree of Masters of Science in **Materials science and engineering**. Therefore, I recommend the submission of a revised version of the thesis to the department following the applicable procedures.

Major Advisor	Signature	Date
Co-advisor	Signature	Date

APPROVAL SHEET

We, the advisors of the thesis entitled **"Synthesis and Characterization of Copper (II) Sulfide & Cobalt Silicate Composites for Enhanced Cationic Dye Degradation from Aqueous Solution"** and developed by Yeshitla Tsegaw Gizaw hereby certify that the recommendation and suggestions made by the board of examiners are appropriately incorporated into the final version of the thesis.

Major Advisor	Signature	Date
Co-advisor	Signature	Date

We, the undersigned, members of the Board of Examiners of the thesis by Yeshitla Tsegaw Gizaw have read and evaluated the thesis entitled **"Synthesis and Characterization of Copper (II) Sulfide & Cobalt Silicate Composites for Enhanced Cationic Dye Degradation from Aqueous Solution"** and examined the candidate during the open defense. This is, therefore, to certify that the thesis is accepted for partial fulfillment of the requirement of the degree of Master of Science in Material science and engineering.

Chairperson	Signature	Date
Internal Examiner	Signature	Date
External Examiner	Signature	Date

Finally, approval and acceptance of the thesis are contingent upon submission of its final copy to the Office of Postgraduate Studies (OPGS) through the Department Graduate Council (DGC) and School Graduate Committee (SGC).

Department Head	Signature	Date
School Dean	Signature	Date
Office of Postgraduate Studies	Signature	Date

ACKNOWLEDGMENTS

First and foremost, I would like to express my gratitude and sincere to my advisor Dr. Dinsefa Mensur Andoshe for his patience, guidance, and very constructive criticism. His guidance helped me in all the time of research and writing of this thesis. I would like to express my deep gratitude to my co-advisor Dr. Osman Ahmed Zelekew for his timely valuable advice and insightful comments. I would like also to express my deep gratitude to Dr. Newaymedehin and Dr. Fikadu Gashaw for allowing me to conduct my thesis experiments in their laboratory center. My thanks also extend to Mr. Demeke Tesfaye, and all staff members of the Materials Science and Engineering department. I would like to express my gratitude to ASTU for giving me this scholarship grant number ASTU/SM- R/214/21 and support by funding my thesis work. Last but not least, I would like to thank my family and my long-time classmates who supported me through their inspiration and advice. Finally, my thanks go to all the people who have supported me to complete the research work directly or indirectly.

TABLE OF CONTENTS

LIST OF TABLES

LIST OF FIGURES

LIST OF ACRONYMS AND SYMBOLS

ABPE	Applied bias photon-to-current efficiency
AGFM	Alternating gradient force magnetometer
AOP	Advanced oxidation process
CB	Conduction band
DMF	Dimethylformamide
DRS	Diffused Reflectance Spectroscopy
EIS	Electrochemical Impedance Spectroscopy
E_g	Energy bandgap
FTIR	Fourier Transform Infrared spectroscopy
Hr.	Hour
hv	Photon energy
HO_2	Per hydroxyl radical
Nps.	Nanoparticles
O_2·	Superoxide radical
OEC	Oxygen evolution catalyst
OH	Hydroxyl radical
PCE	Photo electrochemical
PL	Photoluminescence
PMS	Peroxymonosulfate
SILAR	Successive ionic layer adsorption and reaction
TMC	Transition metal chalcogenide
VB	Valence band
UV	Ultraviolet
UV-Vis	Ultraviolet Visible
XRD	X-ray diffraction
℃	Degree centigrade
ν	Frequency
θ	half Diffraction angle

ABSTRACT

Recently, the removal of dyes from wastewater has become one of the major ways to get treated water. An advanced oxidation process (AOP) has the potential to treat organic dye pollutants wastewater. From the advanced oxidation process, photodegradation by employing semiconductors as a photocatalyst is an attractive method for the removal of organic dye pollutants in wastewater. Among the admired photocatalysts, copper sulfide-based semiconductors are one of the prominent photocatalysts for the degradation of dyes in wastewater industries with low cost, environment-friendly and sustainable treatment technologies for environmental protection. Though CuS was applied as a photocatalyst for the degradation of the dye molecule from wastewater treatment, are still limitations such as recombination in photocatalytic dye degradation performance. Cupper (II) Sulfide (CuS), Cobalt Silicate (Co_2SiO_4), and its composite have been synthesized through the hydrothermal and sol-gel method in which sodium silicate was synthesized from bagasse ash as a silicate source, respectively. The samples were characterized by XRD, SEM, PL, FTIR, and UV- Vis DRS. From the XRD diffraction pattern, it is confirmed the synthesized CuS was crystalline Covellite hexagonal structure with no other impurities peaks where the as-synthesized Co_2SiO_4 were amorphous with a small amount of Co_3O_4. The optical bandgap of the synthesized samples CuS, Co_2SiO_4, and CuS/Co_2SiO_4 -30 were estimated from DRS and PL measurement and were found to be 2.25 eV, 2.5 eV, and 2.5 eV respectively. The photocatalytic performance of the sample was evaluated for each sample, and CuS nanoparticles exhibited low photocatalytic performance of 57% in the degradation of MB, While, the amorphous Co_2SiO_4 shown a higher photocatalytic performance of 93%. The composite of CuS and Co_2SiO_4 exhibited enhanced photocatalytic performance than pure CuS. The experimental results revealed that the (CuS/Co_2SiO_4 -30) composite achieved the highest efficiency of 88 % which is much better than CuS. The efficiencies for the photodegradation of MB dye of the photocatalyst in the CuS/Co_2SiO_4 -30 are stable up to 3rd cycles. Therefore, making a composite between CuS and amorphous cobalt silicate is the best candidate for the degradation of MB.

Keywords: Water pollution, Photocatalyst, CuS, Co_2SiO_4. CuS/Co_2SiO_4 composite and dye degradation

CHAPTER ONE

1. INTRODUCTION

1.1. Background

Environmental pollution caused by industrial wastewater is one of the greatest challenges in the world still now. Industrial wastewater is the aqueous discard that has been dissolved or suspended in water and then it became polluted water. Pollutants in water are broadly categorized as either organic or inorganic [1]. Organic pollutants have become one of the most critical environmental issues because they are non-biodegradable in the environment. Organic pollutants include pharmaceuticals, personal care products, endocrine-disrupting chemicals, pesticides, detergents, and organic dyes are the main contaminant in water [2]. Therefore, those pollutants in our environment need urgent attention and concern due to their high persistence, toxicity, and potential to the bioaccumulation and carcinogenic effect in living things. Traditionally there are various methods to remove pollutants from wastewater such as filtration [3], distillation [4], and sedimentation [5]. It was pointed out that such traditional methods will consume time and leads to sludge. Hence the methods are not sufficient enough for the complete removal of pollutants. There are also other several methods used to treat polluted water, such as adsorption, catalytic oxidation, biodegradation, and photocatalytic degradation.

Adsorption and chemical method is the combined techniques that use the two basic approaches for pollutant removal. From the chemical method, various advanced oxidation processes have been employed to remove organic dyes from water such as photolysis, Fenton, ozonation, sonolysis, photocatalysis, UV photolysis, and wet air oxidation [6]. However, the photocatalysis technique is a process of oxidation and hydrolysis induced by the presence of light and a catalyst without being consumed. Photocatalysis is an advanced, cost-effective technique for wastewater treatment by the complete degradation of the dye pollutants into water, CO_2**,** and nontoxic byproducts [7].

Among transition metal chalcogenides (TMC), copper sulfide (CuS) is one of the important wide direct bandgaps in the range of (1.5 - 2.36) eV semiconductors [8] at room temperature with many excellent physical and chemical properties, which has promising

application in multiple technical fields. It occurs in nature as the dark indigo blue mineral. CuS vary widely in the composition with $0.5 \leq Cu/S \leq 2$, including numerous non-stoichiometric compounds with the formula Cu_xS_y such as CuS_2 (Villamanitite), CuS (Covellite), Cu_9S_8 (Yarrowite), $Cu_{39}S_{28}$ (Spionkopite), Cu_8S_5 (Geerite), Cu_7S_4 (Anilite), Cu_9S_5 (Dignenite), $Cu_{31}S_{16}$ (Djurleite), and Cu_2S (Chalcocite) [9]. Among those segment covellite phases, CuS is one of the most stable IB-VIA transition metal chalcogenides that has acquired a significant interest in current years due to its broad stoichiometric composition and optical bandgap.

Particularly, CuS has been recognized as a fundamental compound for the adaptablescope of applications in; Catalyst and photocatalyst [10, 11], ultrasensitive non-enzymatic glucose sensor electrocatalytic activity [12-15], Nano switches [16], Lithium-ion battery [17-19], Biological application [20, 21] DNA biosensor [22], Vacuum microelectronic industry [23], Electrochemical storage materials and resistive switching devices [24], Optoelectronic devices [25], Solar cell and electronic circuit [26, 27] Electrochemical sensor for detecting cysteine, ascorbic acid [28], Gas sensitivity or Gas sensor [29], Drug delivery system [30], Environmental pollution control [31], and Photovoltaic application[32].

Though CuS was applied as a photocatalyst for the degradation of the dye molecule from wastewater treatment, there is still a limitation. Among these limitations include agglomeration, a high rate of photogenerated charged species recombination, and photo corrosion that means it reacts with the dye molecule to form pollutants by itself. This limitation leads to low photocatalytic performance and stability for the degradation of dye molecules in wastewater. Recent researchers can try to improve those problems by using different techniques. Among them by adding surfactant during the synthesis of nanomaterial to make a quantum dot for minimization of agglomeration, by doping noble metals for twining the bandgap to increase the absorption capacity of sunlight, and by making a composite junction with CuS to minimize the recombination rate and increasing the life span of photogenerated electron and hole pairs to minimize recombination rate.

In addition to CuS, cobalt silicate (Co_2SiO_4) is one of the least studied olivine-type silicates. Because of its high-temperature resistance, it is usually used as a pigment in the ceramic industry. It has a rhombohedral crystal structure and is composed of a compact hexagonal matrix, in which half of the octahedral position is occupied by cobalt atoms. It

is one of the useful electrode materials, with significant theoretical capacity and excellent structural stability [33]. Heretofore, it was being considered to be used as a magnetic material and a catalyst [34-38], and also used as gas sensors [39]. It also exhibits excellent performance for the application of lithium-ion batteries [33, 40-43], hybrid supercapacitors [33, 44-46], and used as photocatalysts [47, 48]. Due to those unique properties of cobalt silicate improve the stability problem and also provide a good charge separation by forming composite to increase the carrier lifetime this decreases the recombination rate problem.

Among AOP methods, photocatalysis is an acceleration of chemical reaction or a change in the rate of a chemical reaction without being the use of catalyst in the presence of light it can be either UV or visible light to boost the reaction. In the presence of light, a semiconductor photocatalyst undergoes the generation of a pair electron/hole but it could only be possible if the energy of light is greater or equal to the bandgap energy of the photocatalyst. In the photocatalytic oxidation process, organic pollutants are destroyed in the presence of a semiconductor photocatalyst, a high-energy light source, and an oxidizing agent such as oxygen or air. Only photons with energies greater than the energy of the forbidden band can cause the excitation of the valence band (VB) electrons, which then promote possible reactions with organic pollutants. The absorption of photons with energy lower than the band-gap energy or longer wavelengths usually causes energy dissipation in the form of heat. The illumination of the photocatalyst with sufficient energy leads to the formation of a positive hole (h^+) in the valence band and an electron (e-) in the conduction band (CB). The positive hole oxidizes either the pollutant directly or water to produce hydroxyl radical •OH, whereas the electron in the conduction band reduces the oxygen adsorbed on the photocatalyst.

In the degradation of organic pollutants, the hydroxyl radical generated from the oxidation of adsorbed water is the primary oxidant, and the oxygen present reacts with the electron at the conduction band to form peroxide radicals followed by many steps forming H_2O_2 or •OH radical thus can prevent the recombination of an electron-hole pair. The •OH attacks organic compounds resulting in various reaction intermediates depending on the nature of the compounds. The resulting intermediates further react with •OH to produce final degradation products such as CO_2 and H_2O [49-51].

Recently, the combination of catalysts and adsorbent magnetic materials has been used as a new method to improve catalytic activity, and anti-photo corrosion performance to achieve efficient recovery and reuse [52]. In this work, we report a composite of CuS and new Co_2SiO_4 that synthesized by hydrothermal and solution method for degradation methyl blue dye through a photocatalytic reaction process. The novelty of this work is synthesizing cobalt silicate from locally extracted sodium silicate solution from waste bagasse ash as silicate source and then making composite with cupper sulfide to boost the dye degradation performance of CuS.

1.2. Statement of the problem

There is still a problem with CuS when we use it as a photocatalyst for the degradation of the dye molecule from wastewater. These problems include agglomeration, a high rate of photogenerated charged species recombination, and photo corrosion that means it reacts with the dye molecule to form pollutants by itself. That problem leads to low photocatalytic performance and stability for the degradation of dye molecules. Recent researchers can try to improve those problems by using different techniques. Among them by adding surfactant during the synthesis of nanomaterial to make a quantum dot for minimization of agglomeration, by doping noble metals for twining the bandgap to increase the absorption capacity of sunlight, and by making heterostructure junction with CuS to minimize the recombination rate and increasing the life span of photogenerated electron and hole pairs. In this work, I synthesized the CuS and cobalt silicate composite from a locally extracted sodium silicate solution from bagasse ash as a silicate source to minimize the recombination rate.

1.3. General objective

Synthesizing and characterizing copper sulfide and cobalt silicate composite photocatalyst for degradation of cationic dye from aqueous solution.

1.4. Specific objectives

- Extracting the sodium silicate solution from sugarcane bagasse ash
- Synthesizing cobalt silicate powder from sodium silicate solution
- Synthesizing the CuS photocatalyst using the hydrothermal method
- Synthesizing the CuS/cobalt silicate composite

- Studying the photocatalytic performance of the synthesized material

1.5. Significance

Water pollution from industrial and disposal effluents in wastewater which have adverse health effects namely pesticides in agriculture, the textile dye in the textile factory, pharmaceutical, and personal care products is still a critical problem in our country.

Therefore, this work was focus on synthesizing and characterizing the CuS photocatalyst and increasing its performance by making cobalt silicate composite to reduce the recombination rate which improves the degradation of the above effluents from polluted water to get treated water and environment.

CHAPTER TWO

2. LITERATURE REVIEW

2.1. Water Pollution

Water is the most important resource that guarantees the survival of all living beings on the earth. It is used for the development of agricultural ecosystems and socio-economic environments for all living things. Water safety is a demanding problem that directly affects animal survival and reproduction and human daily life [53]. Water pollution is defined as, any direct or indirect change in the physical, thermal, chemical, biological, and radioactive properties of any part of the environment through the discharge, emission, or deposit of wastes, thereby affecting useful use or causing danger to the public, any kind the health, safety, or welfare of animals, birds, wild animals, aquatic organisms or plants [54].

Recently rapid urbanization and industrialization have caused both benefits and extensive resource shortage and severe environmental issues, among which water pollution becomes one of the most fundamental and serious problems. It has worsened in the world with numerous hazardous environmental pollutants in water bodies [55]. The major pollution source of water is agricultural and industrial sectors wastes [56], antibiotic waste from hospitals and pharmaceutical companies [57]. Those numerous hazardous environmental pollutants in water bodies are either organic or inorganic. These are various contaminants in wastewater that have diverse health effects for living things includes a textile dye, numerous pesticides, agricultural fertilizer, disinfection by-products, polycyclic aromatic hydrocarbons, polychlorinated biphenyls, and also emerging pollutants such as perfluorooctanoic acid, perfluorooctanoic sulfonate, endocrine-disrupting materials, pharmaceutical, and personal care products are some of the known pollutants for water in the environment [58].

There are various physical, biological, and chemical methods, such as adsorption, chemical precipitation, photocatalysis, chemical oxidation and reduction, electrochemical treatment, that have been used for the removal of dyes from wastewater[59-62]. Among those methods, the photocatalyst is one of the advanced oxidation processes (AOPs) that has progressed rapidly since the discovery of photoelectrochemical water splitting reaction using semiconductors by Fujishima and Honda in 1972 [63]. It has been known as an

environmentally friendly, sustainable, and energy-saving technology. This technology can be applied to low biodegradability, high complexity, and a high concentration of pollutants in the wastewater [64, 65]. These photocatalysts are often referred to as semiconductors. There are many semiconductors which are either metal oxides or metal sulfides that are used for photocatalytic activity includes TiO_2, ZnO, CeO_2, ZrO_2, SnO_2, WO_3, WO_6, $BiVO_4$, $SrTiO_3$, GaP, ZnS, CuS, PbS, and CdS [66-68].

Among the photocatalytic materials, copper sulfide is a chalcogenide chemical compound with a wide range of applications including photocatalysis, solar cells, gas sensors, cathodes in lithium-ion batteries, and thermoelectric materials. It has good stability and catalytic activity at a wide range of pH under visible light wavelength [69]. That has motivated the development of CuS based photocatalysis due to its versatility, availability, and low toxicity and also has a wide range of stable and metastable phases at ambient temperature, ranging from copper-rich to sulfur-rich. Currently, copper sulfide has received particular research attention [70].

So far several various CuS morphologies, including nanorods, flakes, disks, nanowhiskers, nanotubes, nanoplates, urchin-like architectures, trepang-like and flower-like nanocrystals, hollow-spheres, and nanowires have been successfully synthesizing by a different method [71, 72]. These methods include hydrothermal synthesis [73-75], solvothermal synthesis [76-78], thermolysis [79], ultrasonic irradiation [80], microwave irradiation [81], sacrificial templates [82], coordination polymer assembly [83], and electrodeposition [84]. However, among those methods, CuS nanomaterials are synthesized by the hydrothermal route since it has the advantages of controlling the phase, growth, size, and shape of the products [85].

2.2. Crystal structure of CuS

Copper sulfide crystallizes in the hexagonal crystal system in the form of the mineral covellite and whilst these studies are in general agreement on assigning the space group P63/mmc, there are small discrepancies in the bond lengths and angles between them. The structure was described as "extraordinary" by Wells [86] and is quite different from copper (II) oxide but similar to copper selenide (CuSe) (Kockmannite). The covellite phase CuS unit cell contains 6 formula units (12 atoms) in which 2 Cu atoms have trigonal planar coordination and 4 Cu atoms have tetrahedral coordination as shown in Figure.1 (a-b). The two pairs of S atoms are only 2.07 Å apart indicating the existence of an S-S bond (a

disulfide unit). [87-90] The remaining two S atoms from trigonal planar triangles around the copper atomsare surrounded by five Cu atoms in a pentagonal bipyramid (Figure.1 (c)). The S atoms at each end of a disulfide unit are tetrahedral coordinated to tetrahedral coordinated Cu atoms and the other S atom in the disulfide unit (Figure.1 (d) meanwhile the general crystal structure of CuS at above 55 K is shown in Figure. 2.

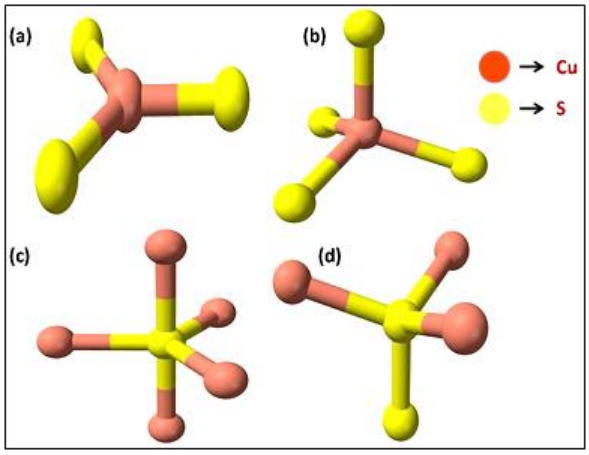

Figure 1. (a-d) (a) Trigonal coordination of copper, (b) tetrahedral coordination of copper (c) trigonal bipyramidal coordination of sulfur, (d) tetrahedral coordination of sulfur-note disulfide unit [91]

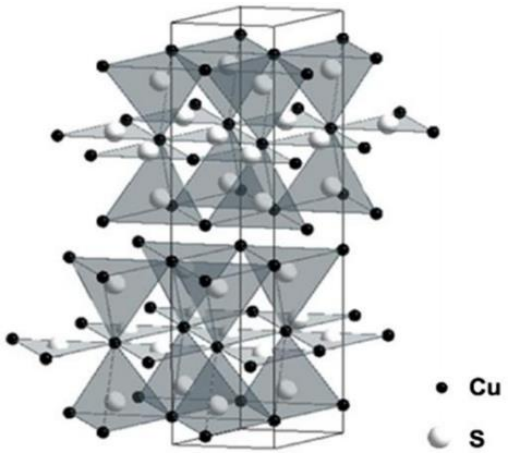

Figure 2. Crystal structure of CuS compound [92].

2.2.1. Lattice parameters CuS

Lattice parameters are considered important when one has to develop for the application of semiconductor devices. Four factors mainly determine the lattice parameters of the semiconductors. (i) Free-electron concentration which affects the potential of the

bottom of the conduction band normally occupied by electrons. (ii) Concentration of impurities and defects and the difference in ionic radii between these defects and impurities concerning substituted matrix ions. (iii) External strains, for example, those induced by temperature. On the other hand, the strict periodicity of the lattice is disturbed by many imperfections or defects. These imperfections or defects have a considerable controlling influence on the mechanical, thermal, electrical, and optical properties of semiconductors. They determine the plasticity, hardness, thermal and electrical conductivities. The lattice constant along the a-axis is 3.799 **Å** and along the c-axis is 16.346 **Å** for the hexagonal form [93].

2.2.2. Optical properties of CuS

Generally, the optical properties of a semiconductor are associated with both intrinsic and extrinsic effects. Intrinsic effects include optical transitions that take place between the electrons in the conduction band and holes in the valence band and excitonic effects due to the Coulomb interaction. External effects are related to dopants or defects that usually produce discrete electronic states in the bandgap, thereby affecting the light emission and absorption processes. Particularly, CuS nanoparticles absorb the radiation in the visible region of 400 to 700 nm, hence CuS host materials are the promising candidate for the application of organic dye degradation in wastewater treatment [94].

2.2.3. Photocatalytic properties of CuS

As a host matrix, CuS being risk-free and economical with stable underneath atmospheric circumstances would be perfect to use in hygienic technology. Moreover, due to its outstanding characteristics and suitable bandgap in the visible region, CuS is identified as one of the best photocatalyst materials. Particularly, CuS nanoparticles absorb the radiation in the visible region of 400 to 700 nm, hence CuS host matrices are the promising photocatalytic materials for organic dye degradation and wastewater treatment [94].

2.3. Photocatalytic Mechanism CuS in the Removal of Dye from Water

Most dyes are synthetic, including anionic such as acid, reactive, direct, cationic, and non-ionic dyes. According to chemical structure, they are divided into azo, anthraquinone, indigoid, nitroso, and nitro dyes. Dyes are frequently used in many industries such as textile, leather, paper, rubber, printing, plastics and they are chemically stable and resistant to degradation after removing waste in the water. This remaining in water for a long time

causes a huge risk to the environment because dyes can reduce sunlight transmission and contain toxic substances, such as heavy metals including lead, chromium, and aromatic compounds [95]. Dyes are the most type of pollutant used for the evaluation of the photocatalytic activity of the catalyst. There are many organic dyes, such as azo dyes including methyl orange, Rhodamine blue, Congo red, acid orange, and cationic dyes including methylene blue [96].

There are different mechanisms for photocatalytic degradation of dyes using photocatalysts as shown in Figure 3 below. These include dye-sensitization through charge injection, indirect dye degradation through oxidation reduction, and direct photolysis of dye [97]. In the dye-sensitization mechanism, the charge carriers such as electron and hole pairs generated in the presence of light can interact with dye molecules through the chemisorption mechanism to produce an exciting dye that can be converted to cationic dye and anionic dye radicals, which leads to degradation products [98].

In the indirect dye degradation mechanism, also when the semiconductor Photocatalyst absorbs photons from solar light with energy equal, or greater than its band-gap, an electron from the valence band is promoted to the conduction band is occurred. This is associated with a hole generation in the valence band to form pairs of electrons and holes participating in reduction and oxidation reactions [99]. The photogenerated electrons and holes trapping in surface states lead to reactions with molecular oxygen to produce anionic superoxide radicals and photogenerated holes react with water forming hydroxyl radicals, which further oxidize the dye molecules to transform pollutants into CO_2, H_2O non-toxic products. The direct photolysis mechanism of dye molecules was a slow process and is independent of the catalysts [100].

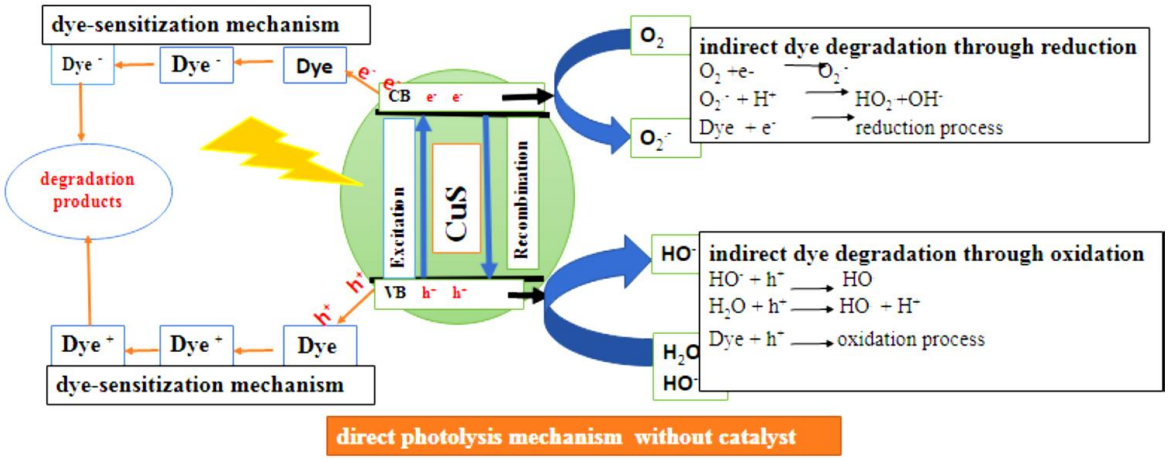

Figure 3. The general photocatalytic degradation mechanisms of dye using a single semiconductor (copper sulfide) light irradiation [101]

2.4. CuS for the Removal of Dye from Wastewater

Copper sulfide (CuS) is a typically p-type semiconductor usually used as a photocatalyst for the degradation of pollutants in wastewater. It has fascinating optical property including a narrow bandgap that shows transmittance in the infrared region and comparatively low reflectance in the visible light region and relatively high reflectance in the near-infrared region [102]. Therefore, CuS is regarded as a promising candidate in the utilization of photocatalyst. However, pure CuS shows a high recombination rate of photogenerated electron-hole pairs producing low catalytic efficiency [103]. Due to this reason, many recent researchers focus on the way to improve that used to enhance the photocatalytic performance of CuS semiconductors by the development of heterojunction structures with at least two advantages: Broadening the photo response variety of the semiconductor substances and enhancing the performance of the separated photogenerated electrons from holes.

2.5. Method to Improve the Efficiency of CuS Photocatalysts

2.5.1. Doping of CuS

Doping is one of the most important techniques to narrow the bandgap of photocatalysts. The narrowing allows the photocatalyst to be active in visible light, thereby enhancing its quantum efficiency and electronic structure kinetics to improve the performance of CuS in photocatalysis. Doping the CuS semiconductor with the transition metals, such as Fe, Co,

and Ni generates new defect locations which work as an electron pond and restrains the photo-generated hole-electrons pair recombination. In consequence, created electrons and holes are shifted towards the catalyst surface where they contribute to reduction reaction with the organic pigment reactive species as well as help in the enhancement of photocatalytic activity. A previous research group has reported that the effect of doping of cobalt, iron, and nickel on photocatalytic performance [104-106]. The cobalt, iron, and nickel-doped CuS samples are synthesized by the facile wet chemical co-precipitation method have shown better photocatalytic activity at 5% Co-doped CuS, 3% Fe doped CuS, and 3% Ni-doped CuS nanoparticle. Predominantly, doped CuS nanoparticles exhibited a significant enhancement of photocatalytic degradation ability because the bandgap of CuS is changed. This consequence of twining leads to the complete degradation of RhB organic pollutants.

A large amount of novel hierarchical flower-like Er-doped CuS had been also successfully synthesized by the facile hydrothermal route [107]. These porous flower-like structures are assembled by many interleaving nanoplates. The presence of Er^{3+} into the hexagonal structure of CuS causes copper vacancies to maintain electro-neutrality. The effect of Er doping into CuS lattice and change of bandgap and defect of catalysts has been investigated by UV–vis–and PL spectroscopy. The introduction of the Er^{3+} dopant into the CuS lattice creates a free hole at the top of the valence band increasing the bandgap. The photocatalytic testing of Er-doped CuS crystals in the MB degradation reaction shows the existence of a maximal rate of methylene blue degradation at Er dopant concentration near 2%. The highest degradation efficiency of flower-like may come from copper vacancies and surface defects would effectively prevent the recombination of photogenerated electron-hole and thus enhanced the rate of degradation. The significant enhancement in photoactivity of the catalyst can be ascribed to the surface defect and copper vacancies. The best durability and activity for the flower-like catalyst can be seen as there is no significant change in the activity even after the third cycle.

In-doped CuS nanostructures were also synthesized by the sonochemical method [108]. In this work due to doping of In into the synthesized nanostructures, the phases are stoichiometric and resulting peaks shifted toward lower angles, and also intensity of the peaks was reduced. The FESEM and TEM images also showed that in the presence of In doping the morphology and the particle size of the synthesized products were changed. The optical features of the samples were changed due to the presence of In doping. The

photocatalytic test also showed that by increasing the concentration of In doping, the degradation level of the MO molecules increased. Photocurrent and EIS have also attracted attention to the photocatalytic degradation of MO with CuS nanostructures.

Table 1. Dyes photocatalytic degradation using various doping on cupper sulfide nanostructure as a photocatalyst

No	Sample	CataList Loading (mg)	dye	Concentration (mg/l)	Pure CuS D%	Doping D%	H_2O_2	Time(min)	Ref.
1	Cu_{1-x} Co_xS Nps x= 0.05	100	RHB	10	74	98	no	60	[104]
2	Cu_{1-x} Fe_xS Nps X= 0.03	100	RHB	10	84.87	98.53	no	80	[105]
3	Cu_{1-X} Ni_XS NPS X= 0.03	100	RHB	10	83.22	98.46	no	60	[106]
4	Cu_{1-x} Er_xS Nps X = 0.02	20	MB	20	60	98	yes	20	[107]
5	Cu_{1-x} In_xS Nps X = 0.03	unknown	MO	unknown	82.8	88.24	no	60	[108]

2.5.2. Composite with Copper Sulfide

To improve the performance of semiconductors in photocatalysis, many heterojunctions/ composites are developed in the last few years. A heterojunction is defined as an interface between two semiconductors with an unequal band structure, according to the different charge carriers' separation mechanisms. Therefore, three types of sulfide-based heterojunction photocatalysis have been reported to date includes straddling gap, staggering gap, and broken gap [101] as shown in Figure 4.

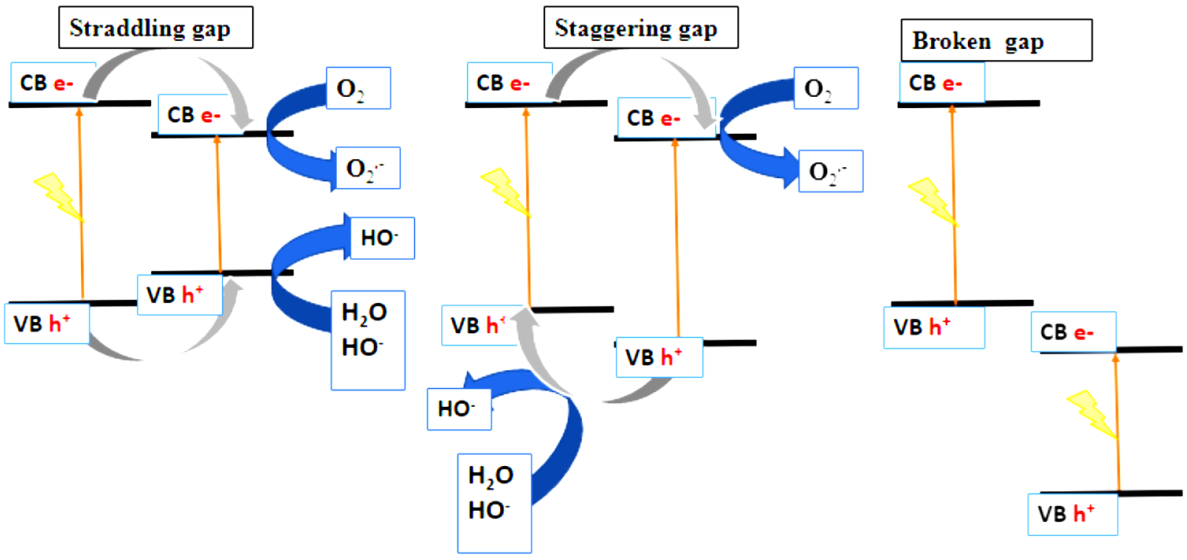

Figure 4.Type of semiconductor heterojunctions based on copper sulfide under light irradiation

By exposure to light on both three types of heterojunctions, semiconductors could be excited to produce photogenerated electrons and holes. In the straddling gap heterojunction, the band energy levels of one semiconductor are included in that of the second one, and the electrons and holes migrate along the same direction. But in staggering gap heterojunction, the electrons and holes are allowed to transfer along the opposite direction to other semiconductors from heterojunction, when spatial charge separation has occurred [109].

Many heterojunction/composites based on copper sulfide nanostructures were developed in the last years; the one reason for the extensive research was to reduce the recombination rate of photogenerated charge carriers, for enhanced performance photocatalytic applications. Among them, the enhanced visible-light photocatalytic efficiency of staggering gap heterojunction ZnO/CuS in MB degradation was also reported [110]. The ZnO/CuS photocatalyst was also obtained by embellishing CuS nanostructure on the surface of ZnO nanotubes, using a wet chemical method at low temperatures.

The photocatalytic experiments showed that ZnO has no photocatalytic activity under Visible light irradiation; the MB photodegradation rate with CuS reaches 63% after 30 min, and with the ZnO/CuS catalyst, the photocatalytic efficiency increased to 87%, meaning an almost 28% increase. Rendering to the mechanism of study, the enhanced photocatalytic activity is endorsed to the ZnO/CuS p-n heterojunction formation, which

favors the efficient separation of photoinduced charge carriers. And also using a simple and eco-friendly hydrothermal method CuS/CdS and CuS/MoS [111, 112] heterojunctions were also synthesized. Based on the photocatalytic results, as compared to pure CuS, CdS, and MoS, the CuS/CdS and CuS/MoS heterostructure showed higher photocatalytic performance toward the degradation of MB dye under Vis-light and simulated natural light irradiation, respectively. It has been stated that CuS/CdS catalyst degraded 99.97% of MB (10 ppm), in presence of H_2O_2 after 10 min of exposure in Vis-light. The CuS/MoS catalyst also totally degraded MB solution of (10 ppm) after 60 min exposure to sunlight. The enhanced photocatalytic degradation efficiencies of CuS/CdS and CuS/MoS photocatalysts are attributed to the significant reduction in the recombination of electron-hole pairs.

The CuS/CuO nanowire heterostructure grown on copper mesh (CuS/CuO/Cu) has been also successfully synthesized by a liquid-solid reaction at room temperature followed by annealing [113]. Among the prepared sample, CuS/CuO/Cu-10, obtained by sulfonating for 10 min with sodium sulfide and then annealing, exhibited the most enhanced photocatalytic activity and good stability in the degradation of MB in the presence of H_2O_2 under visible light irradiation. The degree of degradation of MB reached 87.4% after 20 min and 98.6% after 40 min. The enhanced photocatalytic activity of the CuS/CuO/Cu-10 heterostructure can be attributed to effective electron-hole separation and improved visible light utilization. The photogenerated electrons captured by CuS will react with H_2O_2 on its surface, and the hydroxyl radicals formed will suppress the recombination of electron-hole pairs during the photocatalytic reaction and at the same time, extra holes are produced, which reacts with H_2O to produce more hydroxyl radicals. Therefore, separated electrons on the surface of CuS react with H_2O_2 to afford hydroxyl radicals, which can then react directly with MB. The photostability of CuS/CuO/Cu-10, after repeating the procedure five times remain high, the degree of degradation remained high at 93.7%.

Recently, carbon-based CuS/graphene (graphene oxide) composites are known as very efficient photocatalysts for dyes degradation, due to the graphene (GR)/graphene oxide (GO) specific properties such as large surface area, absorbent morphology, the capacity to photogenerated electrons across the composite interface, and resilient adsorption capacity for organic molecules. In the context of CuS/graphene-based photocatalysts, different heterojunction was prepared and used for the evaluation of MB photodegradation under Vis light irradiation: CuS nanocrystals/GR nanocomposites with different GR weight

ratios (1, 5, 10, and 20)% [114] obtained by the hydrothermal method, flower-like CuS/rGO composites [115] synthesized by a facile one-step solvothermal procedure, and CuS-GO/TiO_2 composites [116] prepared via a sol-gel method. In CuS/GR composites, CuS nanocrystals with an average diameter of 16.2 nm are detached uniformly and completely on GR nanosheets, like bees lying on honeycombs. This porous morphology is suitable for improving light absorption and adsorption of dye molecules. The ability of CuS/GR composites to degrade MB solution, in presence of an oxidant, under UV and Vis light irradiation was investigated. The results showed that the MB degradation efficiency was about 30% higher for CuS/GR (10%) catalyst than that for CuS nanocrystals, after 80 min of irradiation with UV/Vis light, which means a significant increase. The high stability and photoactivity of CuS/GR were assigned to the high electronic conductivity of graphene and its significant influence on the morphology of the CuS/Gr nanocomposite. The photodegradation of MB solutions, without the assistance of H_2O_2 which accelerates the dye degradation, was carried out to evaluate the photocatalytic activity of CuS/GO and CuS/rGO (reduced graphene oxide) based catalysts under visible light irradiation. If in CuS/rGO composites catalysts, CuS micro flowers are uniformly distributed and decorated on the rGO sheets, in CuS/ GO/ TiO_2 catalysts, fine TiO_2 particles are agglomerated randomly on the GO surface.

Generally, high photocatalytic activity is related to uniform particle dispersion on rGO/GO sheets, which is confirmed for CuS/rGO catalyst, and porous morphology, attributed to CuS GO/TiO_2 catalyst due to the pores established on the GO surface. The specific surface areas of a photocatalyst together with micro- mesoporous size distribution have a significant effect on its photocatalytic activity. The rGO sheets, with a high BET surface (34. 8 m^2/g) enhance the specific surface area of CuS/rGO composite by favoring the uniform deposition of more CuS micro flowers on the rGO surface. As a result, the calculated BET surface area was 10.6 m^2/g, almost twice as large as that of pure CuS (5.8 m^2/g). Compared to GO, with a very large specific surface of 1,083m^2/g, the BET surface area drastically decreased to about 3.57 and 13.29 m^2/g for the CuS-GO and CuS-GO/TiO_2 composites, respectively. This decrease was associated with a significant change in microspore size distribution for the CuS/GO/TiO_2 composites compared with that of GO.

The photocatalytic efficiency of CuS/rGO catalyst in MB degradation under visible light irradiation for 140 min was increased to nearly 80% which means about 4 times, respectively two times higher than that of pure CuS and rGO, respectively. After 120 min

under visible light irradiation, the MB degradation efficiency with CuS-GO/TiO_2 catalyst was approximately 33%, 2.3 times higher than that with CuS-GO composite. The enhanced MB degradation efficiency for CuS/GO-based photocatalysts was attributed to the effect of GO in CuS-GO/TiO_2, respectively, rGO in CuS/rGO heterojunction structure, by increasing both the charge mobility of excited photoelectrons to the conduction band of TiO_2/CuS, promoting the efficient charge carrier's separation, and specific surface area (more reactive sites).

A novel hybrid composite 3D CuS-NS/rGO has been synthesized by a simple reduction process to prepare a low-cost aerogel photocatalyst that exhibits remarkable visible-light catalytic activity [117]. This composite catalyst displays prominent morphological leverage of the 3D porous framework as compared to the powdered CuS nanospheres in the spatial separation and transportation of the photoinduced charge carriers. The photocatalytic performance of 3D CuS-NS/rGO composites was studied against the reduction of excellent photocatalytic performance was observed with 3D CuS/rGO hybrid composites as compared to the as-prepared CuS nanospheres. The % removal of 98% for Cr (VI) and 100% for RhB was achieved within 60 min of visible light irradiation. The photocatalytic performance of the 3D CuS-NS/rGO composite catalyst did not decrease significantly with five repeating irradiation times.

Flower-like CuS/UiO-66 composites were also synthesized by a facile solvothermal method [103]. The prepared CuS/UiO-66 composites greatly improved the photodegradation efficiency of RhB. The synergetic effect between CuS and UiO-66 in CuS/UiO-66 composites could transfer electrons effectively and possess a lower rate of electron-hole recombination which facilitated the separation efficiency of photogenerated electron-hole pairs. The CuS in the CuS/UiO-66 composites acted as a sensitizer to absorb visible light. Then, the RhB molecular excited to generate photoinduced electrons, and the photoinduced electrons on the LUMO of RhB could transfer to the LUMO of UiO-66 or the CB of CuS via the dye sensitization effect. Furthermore, the photoinduced electrons on the LUMO of UiO-66 could easily be transferred to the CB of CuS by the closed contact interfaces. It is helpful to improve the photocatalytic ability of the CuS/UiO-66 composites. Due to the above effect, all of the CuS/UiO-66 composites displayed superior photocatalytic activities than pure CuS and UiO-66. What's more, the CuS/UiO-66(2.4:1) composite exhibited the best photocatalytic activity; over 90% of RhB was decomposed in

1h because the catalytic activity depended on the weight ratio of CuS to UiO-66 in the composites and possessed remarkable stability in the catalytic reaction.

Graphitic carbon nitride is an organic semiconductor that could also act as a component of a heterojunction-based CuS photocatalyst. Several studies were focused on the photocatalytic performances of the heterojunction CuS/g-C_3N_4, compared with single CuS and g-C_3N_4 components, in dyes (MB, RhB) degradation under visible light irradiation. The obtaining of the CuS/g-C_3N_4 heterojunctions by a precipitation-deposition method at low temperature, using different amounts of porous g-C_3N_4 (100, 200, and 300)mg, was also reported [118]. The photocatalytic activity of CuS/g-C_3N_4 composites was evaluated for the decomposition of various dyes (RhB, MB) aqueous solutions in visible light irradiation.

In the degradation of MB, the calculated rate constant was 3.57% when CuS/ g-C_3N_4 is used as a photocatalyst, a value which is 21 times or 10.2 times higher than those for g-C_3N_4/CuS. Related to the RhB photodegradation, all the CuS/g-C_3N_4 samples showed enhanced photocatalytic activities compared with g-C_3N_4 (5% degradation efficiency) and CuS (40% degradation efficiency), the highest photodegradation efficiency, after 60 min irradiation in visible light, was about 99.6%. According to this study, the enhanced photocatalytic activity of CuS/g-C_3N_4 heterojunction could be attributed to the matching of the g-C_3N_4 and CuS bandgap energies. As well, high photocatalytic activity and stability in the degradation of RhB dye aqueous solutions under visible light irradiation showed the staggering heterojunction CuS/carbon self-doped g-C_3N_4 nanostructures.

Nanoflowers (NFs) CuS/CCN (carbon self-doped g-C_3N_4) materials were prepared via a mildly hydrothermal method, using different amounts (1, 2, 5, 10 wt. %) of CCN [119]. The variation of CCN content in CuS/CCN samples has a significant influence on the CuS nanoparticle morphology and consequently on the CuS/CCN morphology and photocatalytic properties. According to photocatalysis results, the CuS NFs/CCN (5% wt.) could degrade about 92.6% RhB solution in 180 min, exhibiting a degradation rate of 2.8 times higher than that of CuS NFs. It is obvious that the formation of p–n heterojunctions, with n-type CCN and p-type CuS semiconductors, not only reduces the charge transfer resistance but contributes to the efficient separation of photogenerated electron-hole pairs. Ternary heterostructure composite of Bi_2WO_6/CuS/g-C_3N_4 was synthesized by solvothermal routes is reported [120]. Predominantly this work was solved that the

problem of recombination rate by inhibiting the recombination of photogenerated *e*- and h^+. Also, the ternary heterojunctions can facilitate the interfacial charge transfer and lengthen the migration path of photogenerated charge carriers, which will prolong the lives of active species to engage in photodegradation. Its photocatalytic performance was realized for effective degradation of CIP and RHB 74.94% 75 min and 99.66%, 90 min respectively. It also showed great chemical stability which can degrade CIP nearly the same efficiency after four repeated cycles.

The novel Z-scheme $BiFeO_3/CuS/SiO_2$ heterojunctions Photocatalyst has been also synthesized by hydrothermal routes that are used for the degradation of methyl orange dye [121]. When sunlight hit the surface of the composite both $BiFeO_3$ and CuS were generated the photoexcited charge carriers to form conduction band electrons and valence band holes. The valence band holes of CuS combined with conduction band electrons of $BiFeO_3$ via SiO_2 assisted Z-scheme transference of photogenerated charge carriers, which efficiently hindered the recombining of electrons and holes. In this work, the degradation results revealed that exceptional photocatalytic activity of $BiFeO_3/CuS/SiO_2$ heterojunction Photocatalyst displayed enhanced photocatalytic activity and degraded 90% of methyl orange dye in 60 min and also its recyclability is the same after five repeating cycles.

The ZnO/CuS composite was also successfully prepared by spin-coating, hydrothermal, and SILAR methods [122]. The photocurrent density of the ZnO/CuS composite was higher and the ABPE and IPCE were significantly improved. In all the samples, ZnO/CuS-10 composite displayed the greatest photocurrent density of 1.55 mA cm^{-2} and attained the highest ABPE of 0.368%. All these improvements may be due to the formed p-n heterojunction, depletion layer, and the self–built electric field could improve the transfer rate and the separation of charge carrier. The CuS also acted as a light absorber, captured sunlight, and generated photoinduced electrons. It not only facilitated the transport of electrons but also improved the light absorption ability of composite Thus; the construction of p-n heterojunction is an effective way to enhance the PEC performance and efficiency of charge separation. This work demonstrates that the ZnO/CuS composite has potential applications in Photocatalysis.

A novel immobilized 0D/1D $Au/CuS/CdS/TiO_2$ NBs heterostructure photocatalyst was also designed and fabricated by anodic oxidation, SILAR, and electro-deposition [123].

This heterostructure Plasmonic photocatalyst showed higher photocatalytic efficiency for MOX degradation because this quaternary heterostructure has enhanced utilization efficiency for solar light and higher separation and interfacial transport efficiency for photogenerated electrons. The mechanism to improve the quantum efficiency under irradiation, the electrons were excited and transited in the CB from CuS and CdS to TiO_2 NBs. Under irradiation, the electrons are excited and transited from VB to CB. Due to the potential difference, that is, CB of CuS and CdS is more negative than that of TiO_2, the interface electron transfer is promoted. So, the photogenerated electrons can easily jump in the CB from CuS and CdS to TiO_2 NBs. Meanwhile, photogenerated holes transfer in the VB from TiO_2 NBs to CuS and CdS.

Also, Au NPs were evenly distributed on the surface of CuS/CdS/TiO_2 NBs, which can improve the production and transfer of photogenerated electrons. On the one hand, the Au NPs can act as light sensitizers to enhance light-harvesting efficiency and inject photogenerated electrons to the CB of CuS. On the other hand, the photoexcited electrons accumulated in the CB of TiO_2 NBs can partly inject into Au NPs, which suppresses the electron-hole recombination effectively. The photoexcited electrons located at the CB of TiO_2 NBs and Au NPs can be captured by absorbed O_2 to produce O_2 and also the residual holes in the VB of TiO_2 NBs can yield % OH through reaction with OH^-. Finally, the holes, O_2^- and ·OH radicals all directly or indirectly take part in the oxidative degradation of MOX. The photocatalytic purification effect of MOX by Au/CuS/CdS/TiO_2 NBs photocatalyst was higher than that of its counterparts. Specifically, after the reaction of 60 min, the removal efficiency was 75.4% for Au/CuS/CdS/TiO_2 NBs. The photocatalytic activity of Au/CuS/CdS/TiO_2 NBs has an obvious decrease after three cycles, which may be ascribed to the photo corrosion or photo dissolution that occurred on the surface of the photocatalyst. This paper suggesting that photo dissolution plays the primary role in the photocatalytic activity decrease of Au/CuS/CdS/TiO_2 NBs.

Recently, also the Quantum dots-based CuS based composites have been reported which can enhance photocatalytic efficiency because the composites can separate the photon-generated carrier effectively or change the bandgap of the semiconductor. Herein, the CQDs@CuS nanocomposite synthesized by using a hydrothermal method has been reported [124]. In this work, the CQDs are used as electron donators that could interact with CuS which resulted in the change of band-gap energy of CQDs@CuS nanocomposites. The band-gap energy of the CQDs@CuS was calculated to be 2.25 eV,

which indicated that an easier trend for CQDs@CuS to generate the electron-hole pairs by absorbing a wider wavelength of light. Simultaneously, the lower bandgap was contributed to the separation of electron and hole pairs and inhibition of their regeneration. The change in band-gap energy increased their efficiency to photocatalytic degradation performance of organic dye. The photocatalytic performance of the nanocomposite was improved by CQDs; nearly 99% MB could be degraded in 40 min. The stability and recyclable use of CQDs@CuS composite degradation rate of MB could still reach 92% after five cycle tests. Therefore, the catalysts we synthesized had high stability and a better photocatalytic effect.

Table 2. Dyes photocatalytic degradation using various heterojunctions based on nanostructured copper sulfides as photocatalysts

No	**Sample**	**Catalytic loading (mg)**	**Dye**	**Concentration (mg/l)**	**Composite D%**	**H_2O_2**	**Time (min)**	**Ref.**
1	ZnO/ CuS	20	MB	20	87		30	[110]
2	CuS/CdS	15	MB	10	99.97	yes	10	[111]
3	CuS/ MoS	15	MB	10	99.97	no	60	[112]
4	CuS/CuO/Cu	30	MB	10	87.4	yes	20	[113]
					98.6		40	
5	CuS/graphene	20	MB	80	93	Yes	80	[114]
6	CuS/rGO	0.1	MB	15	80	No	140	[115]
7	CuS-GO/TiO_2	0.2	MB	50	90	No	120	[116]
8	3D CuS /rGO	unknown	MB	10	98		60	[117]
			RHB	10	100		60	
			Cr (VI)	20	98.9		80	
9	CuS/UiO-66	15	RHB	10	90		60	[103]
10	CuS/g-C_3N_4,	10	MB	10	99.6		60	[118]
11	CuS/CCN	20	RHB	10	92.6%	No	180	[119]
12	Bi_2WO_6/CuS/g-C_3N_4	0.01	CIP	10	74.94		75	[125]
			RHB	10	99.66		90	
13	BiFeO3/CuS/SiO_2	unknown	MO	0.5	90		60	[121]
14	0D/1D Au/CuS/CdS/TiO_2	0.89	MOX	5	75.4	No	60	[123]
15	CQDs@CuS	25	MB	20	99		40	[124]

2.6. Cobalt Silicate

Besides CuS, Cobalt silicate (Co_2SiO_4) is one of the less-studied olivine-type silicates that are widely used as, photocatalysts due to its stability against temperatures. It has an orthorhombic crystal structure consists of a hexagonal close-packed oxygen array in which half of the octahedral sites are occupied by cobalt atoms. It is one of the viable electrode materials that possess the considerable theoretical capacity and excellent structural stability [33]. Here to fore, it was being considered to be used as a magnetic material and a catalyst [34-38], and also used as gas sensors [39]. It also exhibits excellent performance for the application of lithium-ion batteries [33, 40-43], hybrid supercapacitors [33, 44-46], and used as photocatalysts [47, 48]. The Co_2SiO_4 nanostructures have been successfully synthesized by various methods including precipitation [126], solvothermal method [127], hydrothermal [33, 48, 128], sol-gel [129].

Co_2SiO_4 nanoparticles were synthesized before via a simple Pechini sol-gel method [47]. In this work, the researcher has investigated the effect of various capping agents on the morphology and particle size of the Co_2SiO_4. AGFM confirms that nanoparticles exhibit magnetic behavior. The photocatalytic behavior of Co_2SiO_4 nanocomposite was also evaluated using the degradation of three various azo dyes under UV light irradiation. The results show that the Pechini method is a suitable method for the preparation of Co_2SiO_4 nanocomposites as a candidate for photocatalytic applications. It also studied that the addition of polymeric nanocomposite for the preparation of Co_2SiO_4 nanoparticles was appropriately enhanced both thermal stability and flame retardant property of the PS and PSU matrices.

A new catalyst for oxygen evolution, amorphous cobalt silicate, was deposited onto the $BiVO_4$ photo anode using a unique photo electrophoretic deposition strategy to achieve a significant improvement in photoelectrochemical performance in water oxidation. Bader's charge analysis revealed that there was an apparent electron transfer from the Cobalt Silicate cocatalyst to the $BiVO_4$ crystal, which effectively limited the starting potential of charge recombination at the interface between the Cobalt Silicate cocatalyst and the $BiVO_4$ photo anode. In addition, the presence of the SiO_4 group in Cobalt Silicate OEC could significantly reduce the free energy of the OOH^* adsorption and thus reduce the over potential of the oxygen evolution reaction which leads to a higher photocurrent density and

a lower starting potential. Photo electrophoretic deposition integrated the processes of electrophoretic deposition and photoelectrochemical activation of the Cobalt Silicate cocatalyst, which led to a higher Co^{3+} / Co^{2+} ratio and thus to an improved catalytic capacity [130].

A cobalt silicate was also synthesized by hydrothermal method using self-sacrificing Indocalamus tessellates leaf-derived silica and investigated as catalysts in sulfate-radical-based advanced oxidization processes for the first time [131]. Co_2SiO_4 presents a unique sandwich structure of a micron-level size acquired from the original leaf template. More importantly, the interior hollow nanotubes assembled by the small nanosheets provide numerous pathways for ion diffusion and remarkably promote mass transport in such large bulk materials. This phenomenon is considered to correlate with the cobalt ion reactivity, size, and recombination rate with SiO_3^{2-}. Co_2SiO_4 exhibits superior catalytic performance that can degrade (MB, 100 mL, 50 ppm) and phenol (100 mL, 20 ppm) within 20 min and 15 min with rate constants of $0.242\ min^{-1}$ and $0.153\ min^{-1}$, respectively, which are comparable to exceed those of the reported PMS catalysts. The key improvements of this work are the successful conservation of the leaf structure after the organic constituent removal; the construction of large-sized Cobalt Silicate catalysts with massive ion diffusion pathways by selecting metal ions and optimizing the reaction conditions, which makes the as-prepared Co_2SiO_4 highly promising and practical in future water treatment.

Even if CuS is a highly photoactive material for absorbing light in visible regions with enhanced solar energy conversion efficiency. But photo-induced electron and hole recombination remain an unsolved problem in a copper sulfide for photocatalyst. In this work, I try to solve the problem by making a composite with new noble amorphous cobalt silicate that is synthesized from bagasse ash as a silicate source.

CHAPTER THREE

3. METHODOLOGY

3.1. Method

The hydrothermal and sol-gel method was used to synthesize photocatalysis. The entire chemical used for the experiment was purchased from BLULUX laboratories, lab tec chemicals, and FINKEM laboratory reagents. All the bagasse ash material was collected from the Wonji sugar factory and the experiments were done in the material science and engineering laboratories at Adama Science and technology university and Addis Ababa university's science faculty, department of physics.

3.2. Materials and Chemicals

Copper chloride dehydrates, $CuCl_2$. $2H_2O$, as Cu source thiourea as sulfur source methylene blue as organic dye molecule, NaOH as sodium source, sugar cane bagasse ash as silicate source, cobalt nitrate as cobalt source, filter paper as filtrate, distilled and deionized water as a solvent and ethanol, distilled and deionized water as washing chemical.

3.3. Preparation of the Sodium Silicate

The Sugar cane bagasse ash was collected from the Wonji sugar factory and it was heated using a furnace for 3 h at 600°C to eliminate carbon content and contaminants. The 5g ash was mixed with 6.5 g sodium hydroxide and the mixture was then calcined at 600°C for 1h. After cooling to room temperature, the fused product was ground and mixed with 200 ml distilled water to form a suspension. The suspension was stirred for 10 h at 80°C using a hot plate magnetic stirrer. Then the mixture was cooled and filtered with filter paper to remove solid residues. The filtered sodium silicate solutions have about a pH of 12 and are used to synthesize Co_2SiO_4.

3.4. Synthesis of Cobalt Silicate

The cobalt silicate was synthesized by procedure was adopted and modified from the literature [130]. The cobalt silicate colloidal solution was prepared by slowly dropping 5 mL of an extracted sodium silicate solution and 5 mL of a 70 mM cobalt nitrate solution

into 80 mL of distilled water under rapid stirring for 1 hour, yielding a bluish violet colloidal solution with a pH of 8.1. For the preparation of the cobalt silicate powder, the cobalt silicate colloidal solution was centrifuged at 5000 rpm for 10 min to form a gel-like cobalt silicate precipitate. After being washed several times with distilled water and alcohol the cobalt silicate precipitate was dried in an oven at 70°C. The dried cobalt silicate precipitate was ground into a powder and calcined at 700 °C for 5 h. and ready for characterization.

3.5. Synthesis of CuS Particles

A typical preparation process for CuS was carried out as follows: 0.04 mole of $CuCl_2$. $2H_2O$ was dissolved in 150 mL of water and then the mixture was heated to 60°C for 30 min with magnetic stirring. Then, 0.16 mole of CH_4N_2S dissolved in 100 mL of water was slowly added into the solution and stirred for 30 min to ensure the good dispersion of the reactants. The final solution was transferred into a Teflon-lined stainless-steel autoclave and maintained at 170°C for 16h and then cooled down to room temperature naturally. The final black products are washed with deionized water and ethanol and dried in a vacuum oven at 50°C for 10 h.

3.6. Synthesis of CuS/Cobalt Silicate Composite

The CuS/Co_2SiO_4 composite with different molar ratios was synthesized as follows, a first certain amount of prepared CuS was dispersed in 30ml dimethylformamide (DMF) by ultra-sonication for 30 min to achieve uniform dispersion. A parallels certain amount of prepared cobalt silicate was also dispersed 30ml dimethylformamide (DMF) by ultra-sonication and the solution is added dropwise into prepared CuS solution then the solution was stirring for 6 hours. Finally, the mixing product was washed several times by distilled water and ethanol and then collected. A series of CuS/Co_2SiO_4 composites with different weight percent of Co_2SiO_4 was fabricated as (10, 20, and 30) % and labeled as (CuS/Co_2SiO_4 -10), (CuS/Co_2SiO_4 -20), and (CuS/Co_2SiO_4 -30), respectively. All the collected product was dried for 12 hours at 70°C in an air atmospheric and the powder was ready for characterization.

3.7. Characterization

The prepared copper sulfide, cobalt silicate, and copper sulfide/cobalt silicate composite were studied by various techniques. To investigate and characterize the phase obtained in

the specimen, the X-ray powder diffraction (XRD) patterns were obtained by a Shimadzu XRD- 7000 with Cu Kα radiation. The morphologies of the samples were also examined by scanning electron microscopy (SEM) model COXIEM-30. UV–Visible diffuse reflectance spectroscopy (DRS) was acquired on a UV-3101 PC Shimadzu spectroscope at room temperature, and $BaSO_4$ was chosen as reference material. FTIR was obtained by an FTIR spectrophotometer measured on Spectrum 65 FT-IR (PerkinElmer) in the range from 4000 to 400 cm^{-1} (resolution: 4 cm-1, number of scans: 4) by using the KBr pellet method. To measure the photoluminescence (PL) spectra of the samples, the PL (VIRAN-CARY ECLIPSE) device with a λ_{exc} = 210 nm, and 250 nm was used. Shimadzu-3600 plus UV-visible spectrophotometer was used for evaluating the degradation of Methylene blue.

3.8. DRS Measurement Procedures

The DRS measurements were recorded between 300 and 800 nm in the absorption and diffuse reflectance modes and transformed to a magnitude proportional to the extinction coefficient through the Kubelka–Munk function (F(R)) for the estimation of the energy bandgap. Spectra were collected at 1 nm intervals with a spectral bandwidth of 2 nm. Before recording the diffuse reflectance spectra, all the samples were mixed with the reflectance reference ($BaSO_4$) in a mortar- at various weight ratios. Powders of the sample with $BaSO_4$ were pressed in holders of 3 cm diameter and 5 mm depth. Nature optical transition of the samples is determined by using the Tauc plot method as shown in Eq.(1) [132].

$$(\alpha h v)^n = K(hv - Eg) \dots\dots\dots\dots\dots\dots\dots\dots\dots\dots\dots\dots\dots\dots\dots\dots\dots (1)$$

Where α is the absorption coefficient, k is a constant, E = hv is the photon energy, Eg is the bandgap energy, and n is the nature of the transition. In photocatalysis; the optical properties of the catalyst play a significant role in the degradation of organic dye. The optical absorption properties, including bandgap for CuS, Co_2SiO_4, and its composites were calculated by direct extrapolation of the reflectance spectra. The UV-Vis diffuse reflectance spectrum from 300 nm to 800 nm wavelength and the corresponding was converted into the absorption mode by using the Kubelka-Munk function. The Kubelka-Munk equation at any wavelength becomes:[133]

$$F(R) = \frac{(1-R)^n}{2R} = \frac{\alpha}{S} \dots\dots\dots\dots\dots\dots\dots\dots\dots\dots\dots\dots\dots\dots\dots\dots\dots.. (2)$$

Where *F(R)*, *R*, *α*, and *s* are Kubelka-Munk function, reflectance, absorption coefficient, and scattering coefficient respectively.

3.9. Photocatalytic Properties Measurement Procedure

100 ml of the methyl blue dye solution (10 ppm) was used as a model pollutant to determine the photocatalytic activity. 0.1 g of CuS, $CoSiO_4$ and CuS/Co_2SiO_4 composite catalysts were used for the degradation of 100 ml solution. The solution was sonicated by a sonicator for 40 min in darkness to determine the adsorption of the dye by the catalyst. The solution was irradiated and stir for 90 min by a 150W tungsten lamp its wavelength is the range between 450 nm to 850 nm which was placed in a quartz pipe in the middle of the reactor. Sampling (about 6 ml) was done every 30 min. The samples were filtered, centrifuged and the dye concentration was determined by UV-Visible spectrometry. The photodegradation efficiency (D %) could be calculated according to Beer-Lambert's law (Eq. (3)), where the concentration of MB is linearly proportional to the intensity of the absorption peak at 654 nm.

$$\boldsymbol{D}\% = \frac{\boldsymbol{Co - Ct}}{\boldsymbol{Co}} \times \mathbf{100} \ldots\ldots\ldots\ldots\ldots\ldots\ldots\ldots\ldots\ldots\ldots\ldots\ldots\ldots\ldots\ldots\ldots (\mathbf{3})$$

Where C_o is the concentration of MB at the initial time and C_t is the concentration of MB at a time after degradation.

CHAPTER FOUR

4. RESULTS AND DISCUSSION

4.1. XRD Analysis

The composition of the synthesized CuS nanoparticles was investigated using XRD, as shown in Figure 5. The obtained patterns with comprehensive peak indexing for CuS nanoparticles are demonstrated in the figure. The CuS nanoparticles were composed of CuS hexagonal phase, well-matched with the standard patterns (JCPDS No. 06-0464). The diffraction peaks observed at 2θ=10.89, 27.24, 27.78, 29.42, 31.92, 32.96, 38.98, 43.26, 43.78, 44.46, 48.00, 52.88, 56.36, 57.38, 58.88, 59.54, 63.58, 67.40, 69.56, 70.18 and 74.26 correspond to the hexagonal phase of CuS and are allocated to the (002), (100), (101), (102), (103), (006), (105), (106), (107), (008), (110), (108), (201), (202), (203), (116), (1010), (118), (0111), (207) and (208) crystallographic planes, respectively. As displayed in the figure the strong and sharp diffraction peaks revealed that the obtained products were well crystallized pure Covellite CuS nanoparticles and no other impurities peaks were observed. The strongest intensity standard diffraction peak (103) indicated that a dominant crystal growth process along the plane (103).

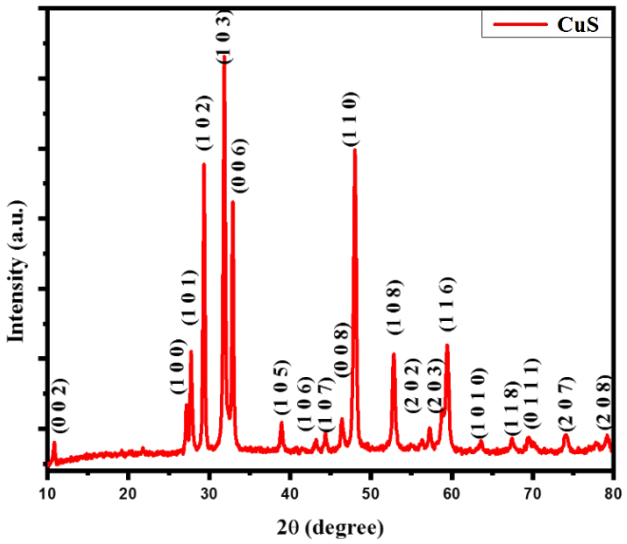

Figure 5. XRD diffraction patterns of CuS nanoparticles

The XRD diffraction of as-prepared Co_2SiO_4 as shown in Figure. 6 (a) is an amorphous-like structure with few wt. % of Co_3O_4. The number of peaks of the phase composition of the sample increased after calcination as shown in fig.6 (b) and became cubic phase of Co_2SiO_4 (JCPDS No. 00-015-0497, space group: F) with a few wt. % of Co_3O_4. The peaks obtained at the 2θ positions 19.37, 31.03, 36.95, 44.83, 56, 65.37, 78.87 corresponds to the (1 1 1), (2 2 0), (3 1 1), (4 0 0), (4 2 2), (4 4 0), (6 2 2) planes of cobalt silicate nanoparticles, respectively. Among the entire obtained peak, the dominated peak is the (3 1 1). The reason for the formation of the Co_3O_4 might be as follows. In the synthesis process, Cobalt silicate-based nanoparticles are resulting from the Co-based precursors by a sol-gel method process in the presence of extract sodium silicate solution. In this process, Co-based precursors will first react with OH that comes from NaOH to form $Co(OH)_2$ first, followed by a small portion of $Co(OH)_2$ being oxidized by O_2 in the air to form Co_3O_4 Eq. (4) [46].

$$6Co(OH)_2 + O_2 \rightarrow 2Co_3O_4 + 6H_2O \quad (4)$$

$$SiO_2 + 2OH^- \rightarrow SiO_3^{2-} + H_2O \quad (5)$$

$$2Co(OH)_2 + SiO_3^{2-} \rightarrow Co_2SiO_4 + H_2O + 2OH- \quad (6)$$

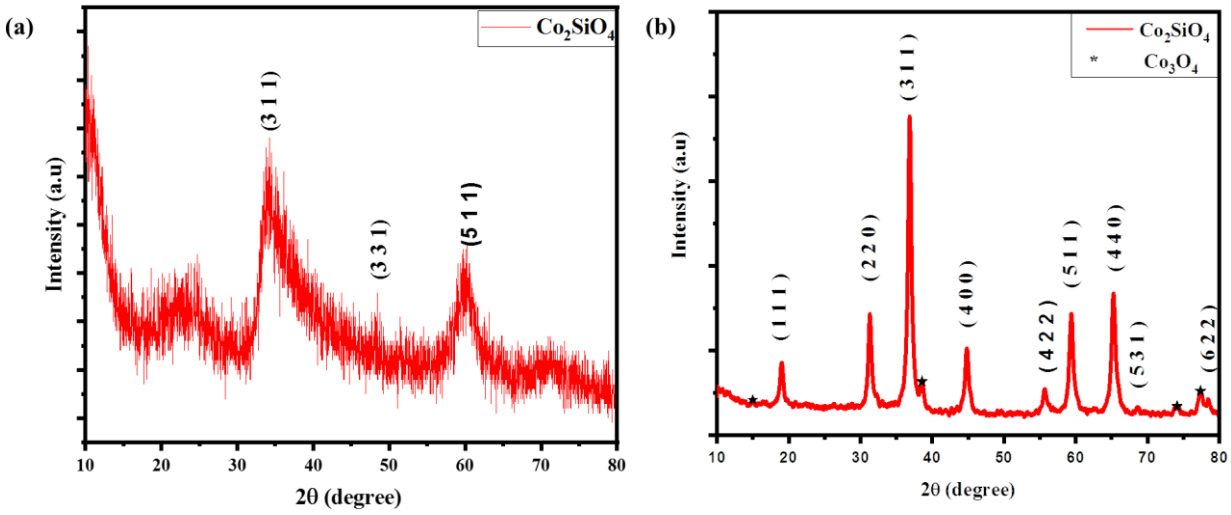

Figure 6. XRD diffraction patterns of cobalt silicate nanoparticles prepared from bagasse ash as a silicate source (a) as-prepared (b) calcined at 700 °C for 5 hrs.

Figure 7 shows that the phase compositions and crystal structures of the CuS/Co_2SiO_4 composites were studied with XRD; No other peaks other than those characteristics of CuS could be seen. The crystallinity of CuS is retained in the nanocomposites, as demonstrated by the XRD patterns, which indicate that the addition of amorphous cobalt silicate into CuS does not change the crystal orientations of the CuS composites.

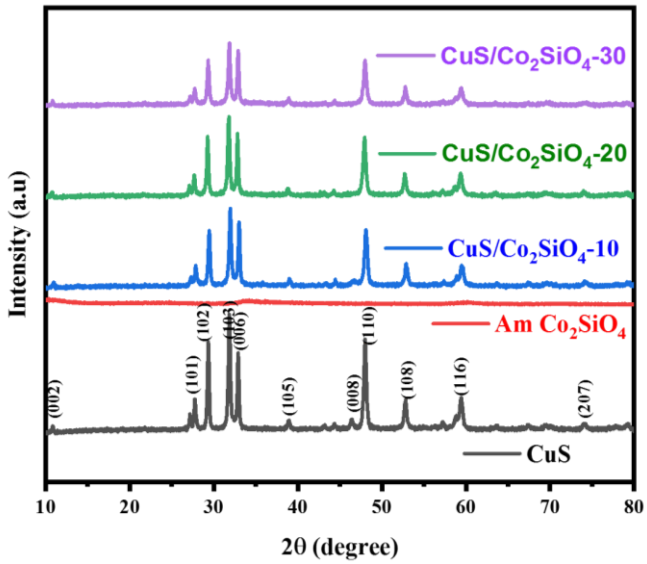

Figure 7. XRD diffraction patterns of CuS, amorphous Co_2SiO_4, and CuS/Co_2SiO_4 composite at a different molar ratio

The average crystalline size of cupper sulfide, cobalt silicate, and its composite was also calculated by the Scherrer equation as shown in Eq. (7) [134].

$$\boldsymbol{D} = \frac{\boldsymbol{k\,\lambda}}{\boldsymbol{\beta * cos\theta}} \ldots \ldots \ldots \ldots \ldots \ldots \ldots \ldots \ldots \ldots \ldots \ldots \ldots \ldots \ldots \ldots \ldots \ldots \ldots \ldots \ldots .. (\mathbf{7})$$

Where β is the width of the observed diffraction peak at its half maximum intensity (FWHM), K is the Scherrer constant about 0.9, and λ is the x-ray wavelength (Cukα radiation, equals 0.154 nm).

Table 3. The calculated average crystal size of synthesized copper sulfide, cobalt silicate, and its composite is provided in the given below.

Samples	**D (nm)**
CuS	33
Co_2SiO_4	26
CuS/Co_2SiO_4 – 10	29
CuS/Co_2SiO_4 – 20	30
CuS/Co_2SiO_4 – 30	36

Table 3, is displayed the average crystal size of synthesized copper sulfide, cobalt silicate, and its composite. When we increase the composition of cobalt silicate on CuS, the crystal size of the composite increased from 29 to 36 nm because it might be due to the adsorption of cobalt silicate on the surface of CuS.

4.2. DRS for Optical Bandgap Determination

The diffuse reflectance spectra of CuS, Co_2SiO_4 nanoparticles and their composite were measured at room temperature. The samples showed a minimum reflectance in the visible region. This indicates the photons with higher energy absorbed by the sample. The optical band gap of optically active materials can be estimated from a plot of $(F(R)\ hv)^2$ versus

photon energy. The extrapolation to the energy axis whose intercept to the x-axis gives the optical bandgap [135], and the optical bandgap of the synthesized sample was estimated as shown in Figure 8 (a-e) below.

The Eg of pure CuS is 2.25 eV and the Eg of as-synthesized cobalt silicate is also 2.5 eV as shown in Figure 8(a) and (b). When making composites with each other its bandgap is increased to the bandgap of 2.75 eV for (CuS/Co_2SiO_4 -10) as shown in Figure 8 (c). Then after further adding of the synthesized cobalt silicate with increasing the Co_2SiO_4 weight percent, the bandgap of the composite decrease from 2.75 to 2.6 eV, 2.5 eV for (CuS/Co_2SiO_4 -20), and (CuS/Co_2SiO_4 -30), respectively as shown in Figure 8 (d) and (e).

The bandgap of the composite decreased with increases in the composition of cobalt silicate might be due to the increase of crystal size of the material. In simple words electrons are not confined i.e., occupied more space as crystal size increases, hence VBM and CBM potentials are shifted less +ve and -Ve respectively, resulting in the small bandgap. These results suggested that the optical absorption properties of CuS would be enhanced after modifying with amorphous Co2SiO4 and hence could be a promising photocatalytic material in the visible light region.

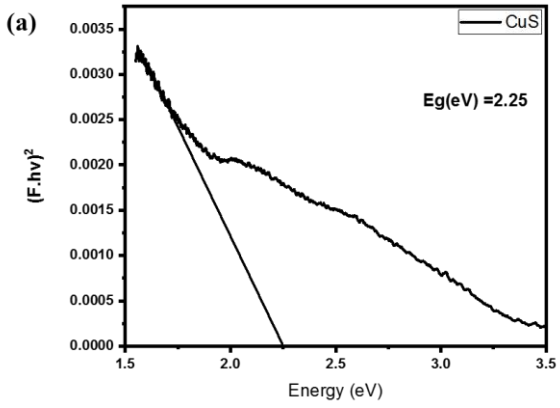

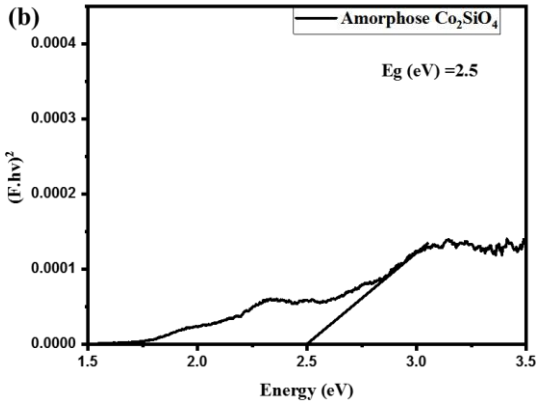

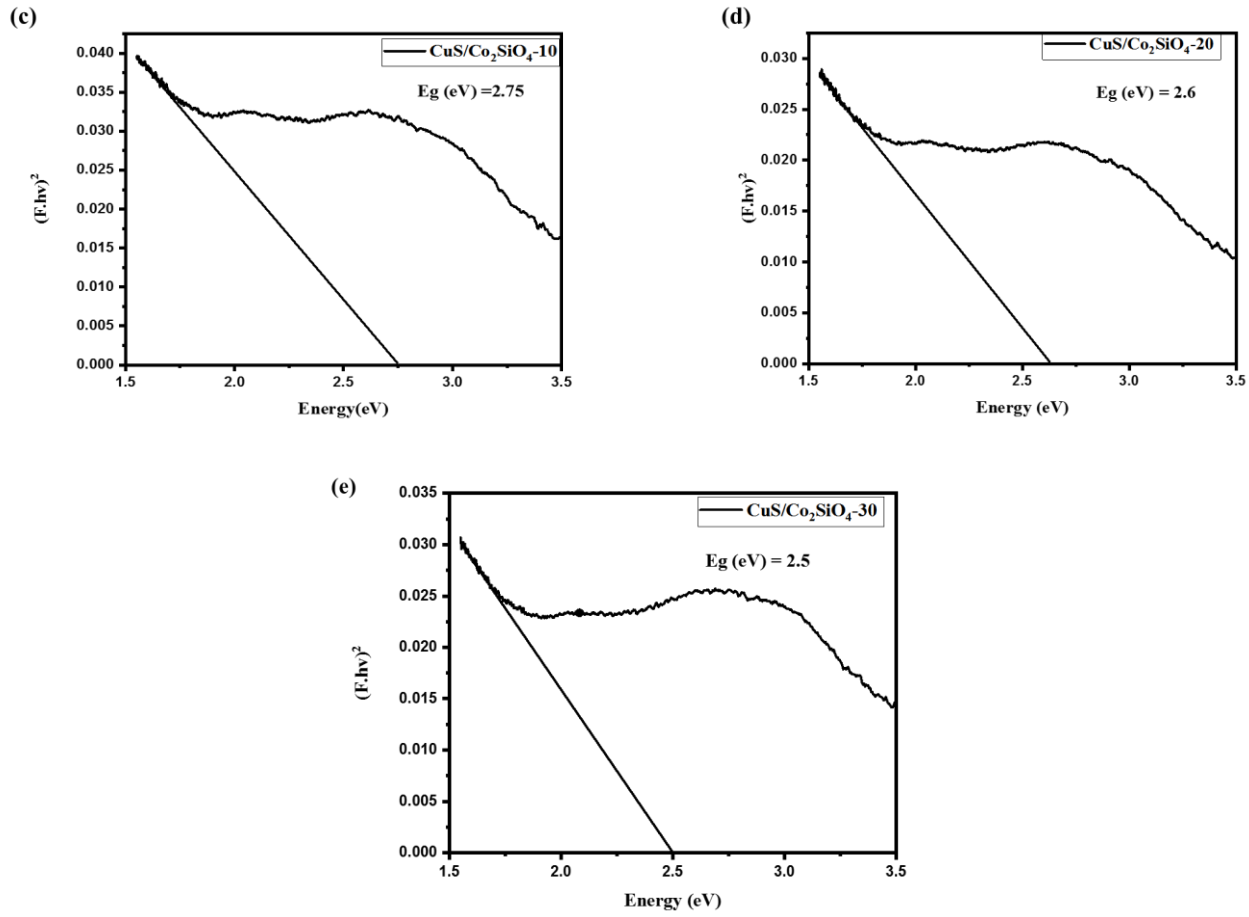

Figure 8. (F (R_∞) hv) ^{2} vs energy plot for estimating the optical bandgap (a) CuS, (b) Co_2SiO_4, (c) CuS/Co_2SiO_4-10, (d) CuS/Co_2SiO_4-20, (e) CuS/Co_2SiO_4-30

4.3. Morphological Analysis

The morphologies of the synthesized sample were examined by SEM. The SEM image of the synthesized CuS revealed that many flowerlike CuS architectures were formed, as shown in Figure 9(a). Amorphous cobalt silicate displays severe agglomeration, leading to dense and larger irregular porous structures, as shown in Figure 9(b), which will improve the kinetics of adsorption reaction. The SEM image revealed that the calcined Co_2SiO_4 were clusters of the random shape of rectangular and octagonal morphology as shown in Figure 9(c). The CuS/Co_2SiO_4 -30 composite exhibited some individual and entangled cobalt silicate on the surface of the CuS micro flower-like structure, as shown in Figure 9(d). It appears that many cobalt silicates were embedded between the flower structures on one end, while they were

exposed to the surface on the other. Moreover, energy dispersive spectroscopy (EDS) analysis was performed to evaluate the average elemental composition of cobalt silicate. The EDS pattern confirmed that the presence of Si, Co, and O elements, and that there were no other peaks that would indicate the presence of impurities as shown in Figure 9(e).

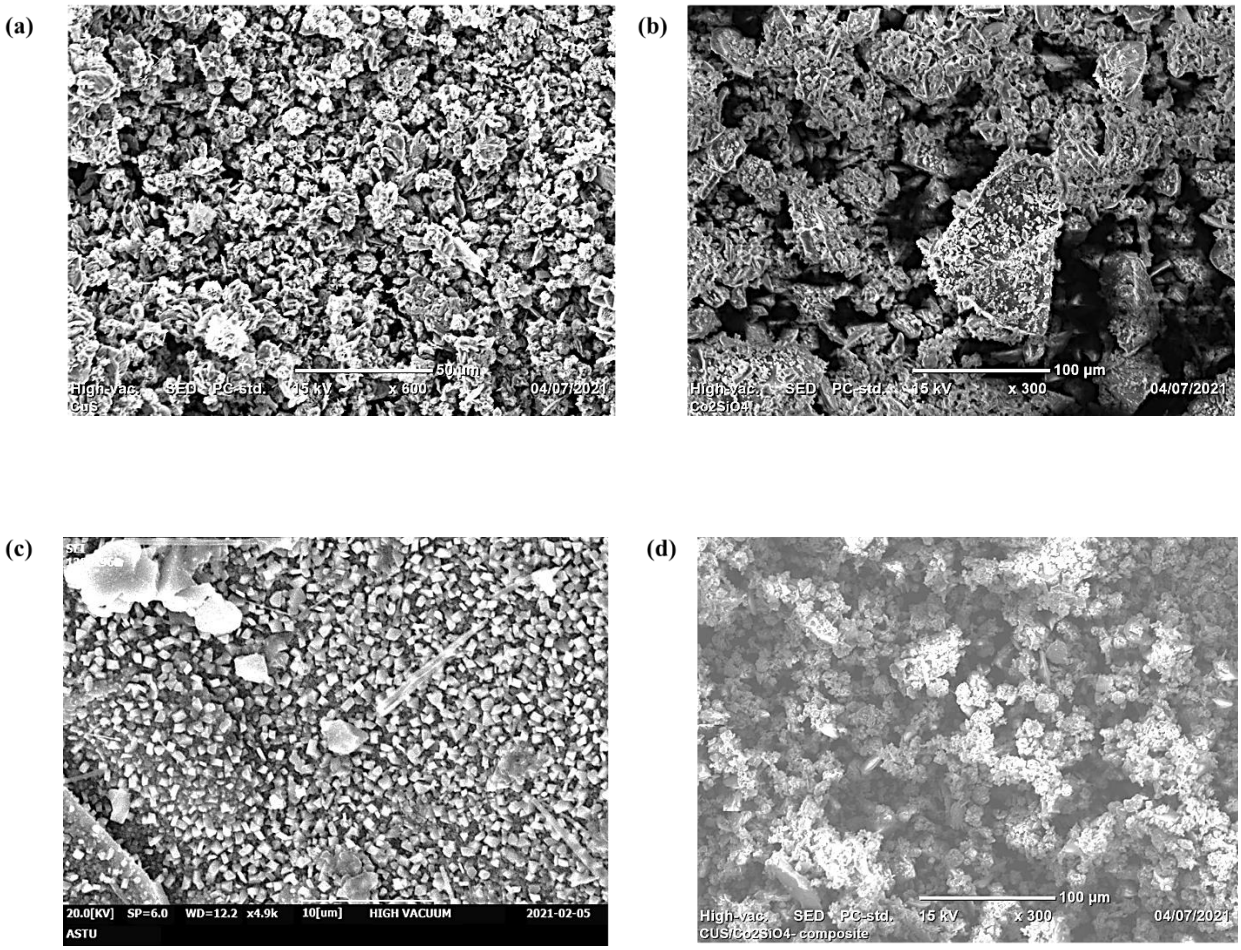

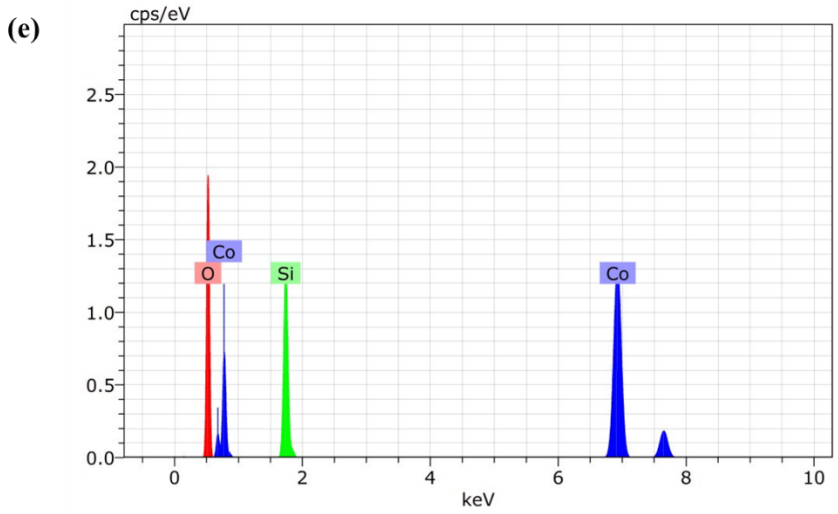

Figure 9. SEM images of (a) CuS, (b) Amorphous cobalt silicate, (c) calcined cobalt silicate, (d) CuS/cobalt silicate composite (e), and The EDS elemental composition cobalt silicate catalyst.

4.4. FTIR Analysis

The bonding groups prove the formation of CuS, Co_2SiO_4, and its composites are confirmed by FT-IR spectroscopy. The FT-IR spectra of the synthesized CuS, Co_2SiO_4, and the composites are taken in the range of 4000-400 cm^{-1} at room temperature as shown in Figure 10 (a). The FT-IR of CuS shows strong absorption peaks at 3584 and 1674 cm^{-1}, which recognized the stretching and bending vibration of O–H groups of adsorbed water molecules [136]. The other peaks in the CuS are located at, 1510, 1180, and 532 cm^{-1}. Which correspond to C–OH, C–C, and CuS stretching vibration modes respectively [137].

In Figure 10 (b) The FT-IR of Co_2SiO_4 also shows strong absorption peaks at 3586 and 1667 cm^{-1} which indicating the stretching and bending vibration of O-H groups of adsorbed water molecules and the other peaks located at 1478, 994, 643, and 451cm^{-1}. These peaks are related to the bond vibration of SiO_4 tetrahedron, the vibration of the Si-O-Si bond, the vibration of the OH-3Co group and the stretching vibration mode SiO, and the asymmetric bending vibration Si-O, respectively [138]. Figure 10 (c) The FTIR of CuS/Co_2SiO_4 -30 composite also has been shown absorption peaks at 3581 and 1686 cm^{-1} which also indicate the stretching and bending vibration of O-H groups of adsorbed water molecules in the sample. The other peaks

1476, 997, and 467cm^{-1} in the composite shows that the vibration bond of SiO_4 tetrahedron, the vibration of the Si-O-Si bond, and the stretching vibration modes CuS, respectively.

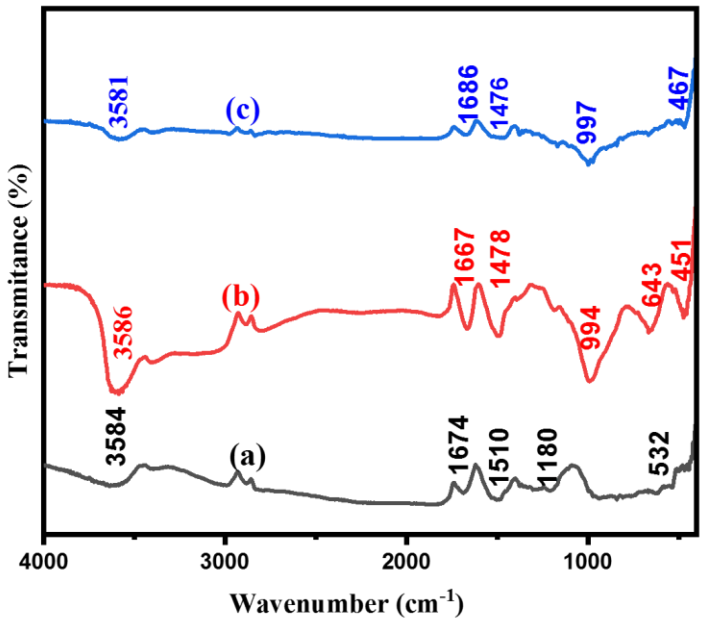

Figure 10. FT-IR spectra of the synthesized; (a) CuS, (b) Amorphous Co_2SiO_4, (c) CuS/Co_2SiO_4 -30

4.5. Photoluminescence (PL) Analysis

The photo luminescent (PL) activity of CuS, Amorphous Co_2SiO_4, and CuS/Co_2SiO_4 composites at room temperature shown in Figure 11 has been investigated to determine the surface vacancies, transfer, and recombination of photo-generated electron-hole pairs in photocatalysts. The PL spectra of CuS exhibited emission peaks in the 550 and 567 nm region under an excitation wavelength of 250 nm, which was mainly due to the bandgap and the surface defects of CuS lattice or the interstitial Cu defects [139]. The PL spectra of amorphous Co_2SiO_4 also exhibited emission peaks in the 482 and 526 nm region under an excitation wavelength of 210 nm, which was maybe due to the formation of Co_3O_4 impurity and the amorphous nature of cobalt silicate. It was also believed that morphology, size, and crystalline had an important effect on the emission spectrum. Furthermore, the PL intensity of CuS/Co_2SiO_4 has exhibited an emission peak at 480 nm which shows that the photogenerated

charge carriers have low efficiency of recombination in CuS/Co_2SiO_4 composite due to the loading effect of Co_2SiO_4. Therefore, the enhanced photocatalytic performance of CuS/Co_2SiO_4 can be achieved due to the low efficiency of recombination of hole-electron pairs.

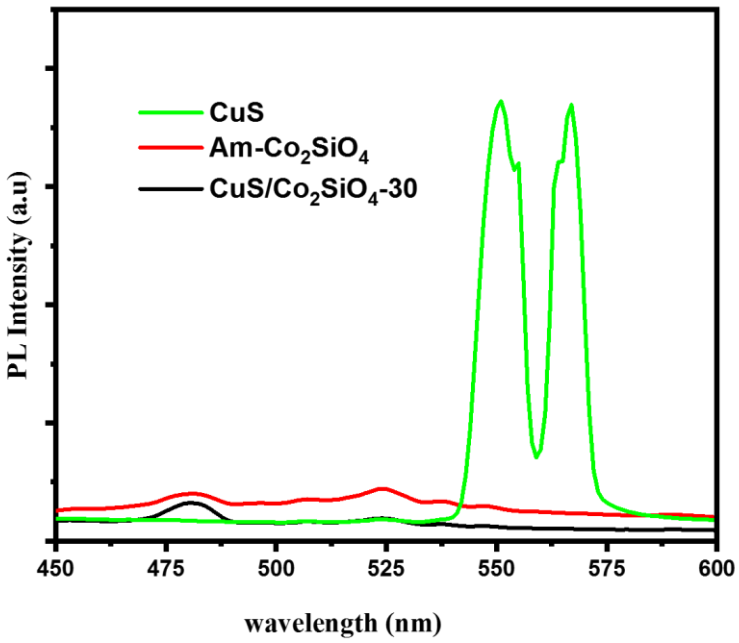

Figure 11. PL spectra of synthesized CuS, Amorphous Co_2SiO_4, and CuS/Co_2SiO_4 -30

4.6. Photocatalytic Dye Degradation

Visible light photocatalytic activity experiments were conducted at room temperature by irradiating a 150 W tungsten halogen lamp light source to discoloration of MB in an aqueous solution. The discoloration performance of CuS, amorphous Co_2SiO_4, and its composites such as CuS/Co_2SiO_4 -10, CuS/Co_2SiO_4 -20, and CuS/Co_2SiO_4-30 were measured using UV-visible spectroscopy in the range of 200-800 nm. The solution was first sonicated for 40 min and then irradiated and stir for 90 min by a 150 W tungsten lamp its wavelength is in the range between 450 nm to 850 nm which was placed in a quartz pipe in the middle of the reactor. Sampling (about 6 ml) was done every 30 min and measured by UV-Vis Spectra spectroscopy. The UV-

Vis absorption spectra of MB solution at different time durations of CuS, Co_2SiO_4, and CuS/Co_2SiO_4 composite samples were depicted in Figure 12 (a-e) below.

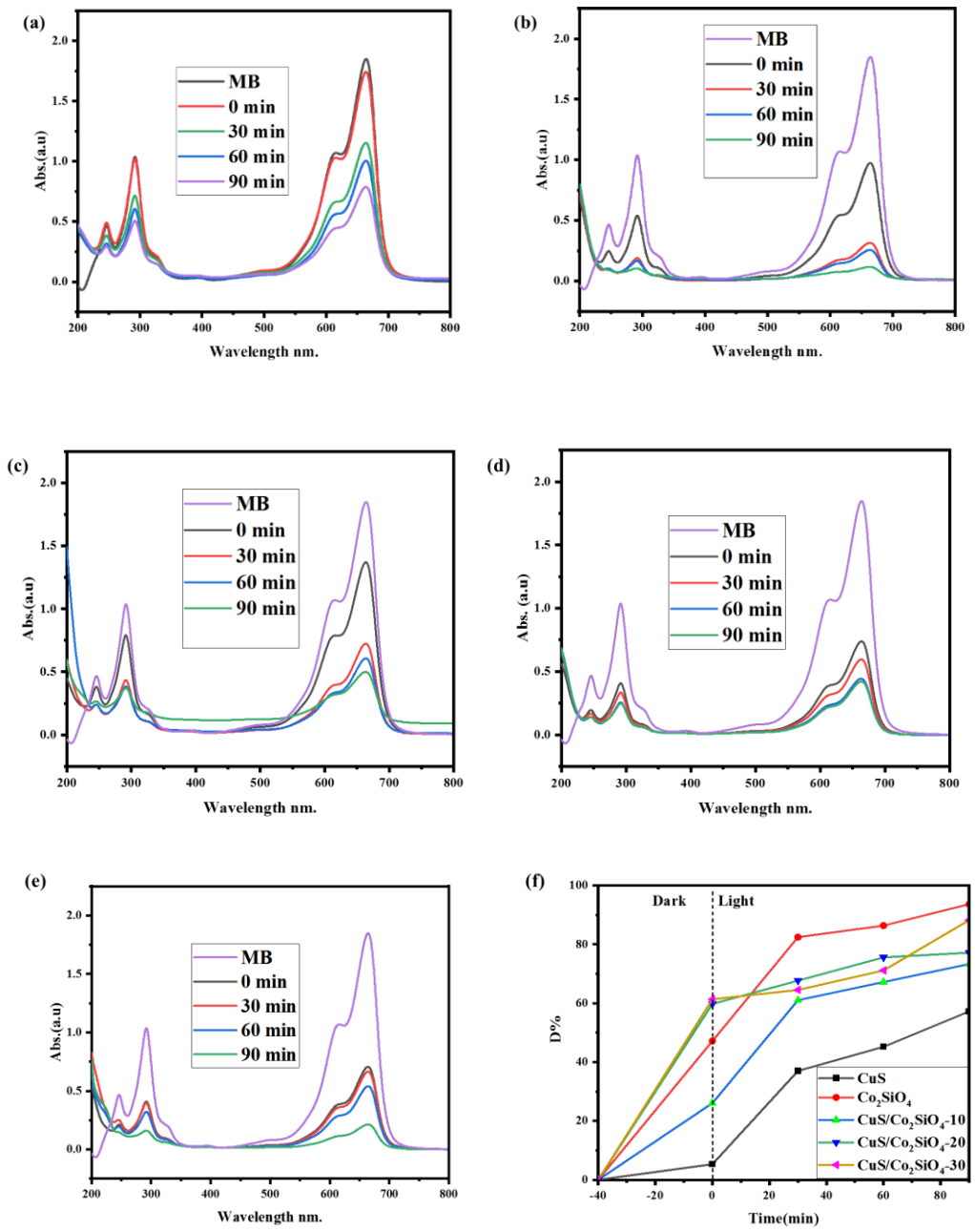

Figure 12. UV-Vis absorption spectra of MB solution at different light exposure time durations of (a) CuS, (b) Amorphous Co_2SiO_4, (C) CuS/Co_2SiO_4-10, (d) CuS/Co_2SiO_4-20, (e) CuS/Co_2SiO_4-30, and (f) the degradation performance of MB by each sample

Figure 12 (a-e) shows the decrease in the intensity of the 664 nm absorption peak was followed and evaluated to study the degradation of methylene blue under visible light over different time intervals. As the irradiation time increases, the peak at 664 nm declines in intensity indicating the degradation of MB. Upon further light exposure, the absorption peak intensity drops rapidly with time. The photocatalytic performance of CuS, Amorphous Co_2SiO_4, and its CuS/Co_2SiO_4 composite was examined by the degradation of MB as shown in Figure 12 (f). Amorphous cobalt silicate shows superior photocatalytic performance comparing with all samples for the degradation of MB, which degraded 93% of MB in 90min. Figure 12 (b) shows the amorphous Co_2SiO_4 has a high dye adsorption ability during dark reaction probably due to its amorphous structure that may increase specific surface area to adsorb MB and also has a photocatalytic effect due to Co_3O_4 impurity that forms during the reaction to form Co_2SiO_4 nanoparticles as shown in Figure 6 (a) [46].

The CuS shows low photocatalytic performance as shown in Figure 12 (a) due to its photogenerated charge carrier recombination and optical band gap, which degrades 57% of MB. Strikingly, making CuS/amorphous Co_2SiO_4 composite greatly improved the degradation efficiency of MB. Because of increasing the loading amorphous Co_2SiO_4 the adsorption effect of the composite is an increase during a dark reaction. Due to the effect of loading amorphous Co_2SiO_4, All the CuS/Co_2SiO_4 composite (10, 20, and 30) displayed superior degradation activities of MB with the value of 73%, 77%, and 88%, respectively than that of pure CuS. What's more, the CuS/Co_2SiO_4–30 composite exhibits the best degradation activity, over 88% MB was decomposed in 90 min. It could be inferred that in CuS/Co_2SiO_4 –30 composite, both CuS and Co_2SiO_4 may be used as a cocatalyst that is in close contact with each other. This could greatly improve the separation rate of photoexcited electrons and holes, so the photocatalytic activities of the composite were higher than that of pure CuS particles.

Table 4. Overall summary of photodegradation performance of the synthesized sample at different time intervals.

Time (min)	Percent of degradation of MB (D %)					
	MB	CuS	Am Co_2SiO_4	CuS/Co_2SiO_4-10	CuS/Co_2SiO_4-20	CuS/Co_2SiO_4-30
0	0	5.30556	47.17721	26.06151	59.77179	61.34171
30	0	37.02558	82.46592	61.02803	67.69796	64.51983
60	0	45.20294	86.35319	67.19859	75.58585	71.14413
90	0	57.22163	93.63149	73.31503	77.15577	88.22178

4.7. Kinetics Study

As can be seen from Figure. 13 (a), the photodegradation rates of MB were faster with CuS/Co_2SiO_4 composite than pure CuS under the same condition. The kinetic degradation of MB dye photodegradation at neutral pH using CuS, amorphous Co_2SiO_4, and CuS/Co_2SiO_4 composite was studied based on the pseudo 1st order modal as in Eq. (8) [7].

$$-\boldsymbol{ln}\frac{\boldsymbol{Ct}}{\boldsymbol{Co}} = \boldsymbol{Kt} \ldots\ldots\ldots\ldots\ldots\ldots\ldots\ldots\ldots\ldots\ldots\ldots\ldots\ldots\ldots\ldots\ldots\ldots\ldots\ldots\ldots . . (\boldsymbol{8})$$

Where C_t is the concentration of MB at irradiation time t, C_0 is the initial concentration before irradiation, K is the1st order rate constant (min^{-1}). Then plotting ln (C_t/C_o) vs t as shown in Figure. 13 (b) and the value of reaction rate is exhibited in Figure. 13 (c) was calculated for CuS, amorphous Co_2SiO_4, CuS/Co_2SiO_4 -10, CuS/Co_2SiO_4 -20, CuS/Co_2SiO_4 -30 to be 0.0086, 0.02563, 0.01285, 0.01212, and 0.01671 min^{-1}, respectively. Co_2SiO_4 presents a higher kinetic rate than pure CuS and the introduction of Co_2SiO_4 can further increase to some extent. The data fitted well and gave a correlation coefficient of CuS, amorphous Co_2SiO_4, CuS/Co_2SiO_4 -10, CuS/Co_2SiO_4 -20, and CuS/Co_2SiO_4 -30 to be 0.96449, 0.9195, 0.87749, 0.62164, and 0.77111, for neutral pH respectively.

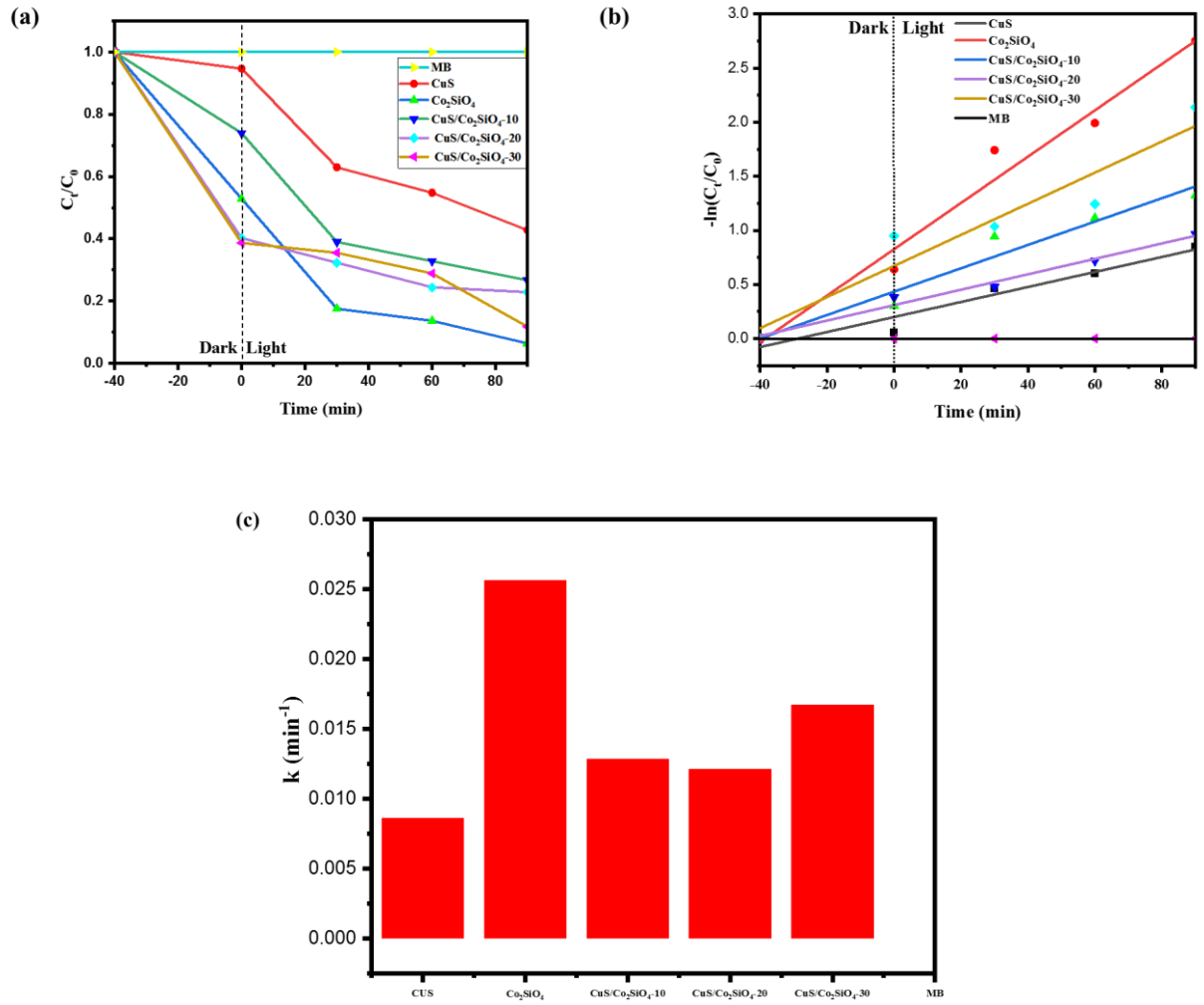

Figure 13 (a) The variation of MB concentration under visible irradiation at different periods, (b) the consistent reaction kinetics of photodegradation of MB, (c) the reaction rate constant of CuS, Amorphous Co_2SiO_4, and different CuS/Co_2SiO_4 catalysts

4.8. Dye Degradation Mechanism of CuS/Co_2SiO_4 Composite

During the dark reaction, the adsorption ability of cobalt silicate towards MB is higher due to its amorphous-like nature of synthesized cobalt silicate. These Co_2SiO_4 amorphous surfaces provide enhanced adsorption capacity to the composites by the presence of the Co_2SiO_4 active surfaces on CuS. Adsorption ability of amorphous Co_2SiO_4 may support the deposition of the MB during dye degradation by CuS. During light reaction when the CuS/Co_2SiO_4 catalyst absorbs light in the visible region, and e^- / h^+ pair will be generated; upon light absorption,

electron excited from valance band to conduction band of CuS resulting in the generation of electron/hole pair. The electron in the CB of CuS could easily transfer to the surface of Co_2SiO_4 decorated on CuS and further, reduce O_2 absorbed on the surface to $\bullet O_2^-$, which had sufficient oxidizing ability to degrade MB dye during photocatalytic reactions, as a consequence, Co_2SiO_4 was served as an electron mediator to effectively separate and transfer electron-hole pairs, which greatly promoted the photocatalytic MB degradation property of due to CuS/Co_2SiO_4 interfacial catalytic active sites. Meanwhile, the photogenerated holes from the valence band break H_2O and lead to the formation of •OH radicals, hence, in turn, degrading the MB dye molecules. Thus, with a visible light source using CuS/Co_2SiO_4 catalyst, large amounts $\bullet O_2^-$ and •OH are generated which enhances the degradation of the methylene blue dye. The photogenerated electron of CuS is captured and transferred by Co_2SiO_4 surfaces, which may be thereby reducing the recombination rate of photoelectron-hole pairs. Overall, the photocatalytic efficacy of the prepared composite is due to the synergetic effect of Co_2SiO_4 and CuS.

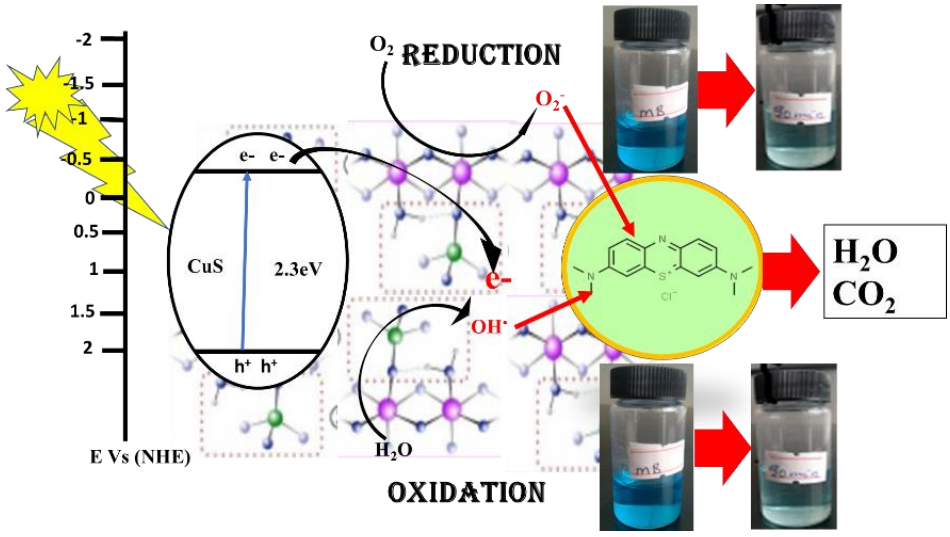

Figure 14. Schematic diagram of the proposed reaction mechanism for MB degradation with CuS/Co_2SiO_4 composite

4.9. Stability and Recyclability

Reusability and stability are further vital considerations for the valuation of the composites because photo corrosion will affect their stability. The photocatalytic stabilities of the composites were assessed by recycling them from their aqueous systems and reusing them in

repeated MB degradation experiments (Figure 15). This Figure shows that up to 88% of MB is degraded after 90 min in the first cycle of degradation and MB degradation could be observed in the second to fourth cycles was 87%, 80%, and 50%, respectively. Thus, the efficiencies for the photodegradation of the photocatalyst in the CuS/Co_2SiO_4 -30 photocatalyst are stable to MB dye degradation. Reused in third cycles are nearly the same. But in the fourth cycle, the degradation is decreased to 50%. Thus, the CuS/Co_2SiO_4 -30 photocatalyst is stable for MB dye degradation for up to 3-cycles.

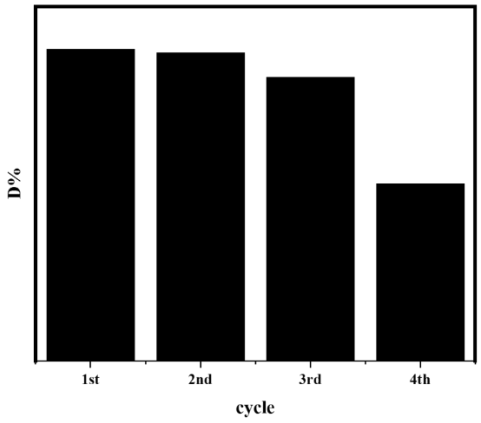

Figure 15. The cycle runs of CuS/Co_2SiO_4 -30 composite for degradation of MB degradation under visible light radiation

5. CONCLUSION

The CuS, amorphous Co_2SiO_4, and CuS/Co_2SiO_4 photocatalyst were successfully synthesized by hydrothermal, sol-gel, and solution method respectively and characterized their crystallographic properties were characterized by XRD, the morphology by SEM, the distinctive molecular fingerprint by FTIR, and the optical properties by PL, DRS using UV-VIS spectroscopy. The XRD results confirm that the synthesized CuS was pure CuS nanoparticles. The XRD study of the prepared Co_2SiO_4 revealed that amorphous Co_2SiO_4 with few percentages of Co_3O_4. The optical bandgap of the synthesized sample was estimated from DRS measurement. The photocatalytic dyes degradation performance of the synthesized sample was also measured using methyl blue under visible light irradiation. Amorphous Co_2SiO_4 prepared from extract sodium silicate solution from bagasse ash was a superior photocatalytic performance for the degradation of MB, which degraded 93% of MB in 90 min. All composites exhibit higher photocatalytic activity than that of pure CuS for degradation of MB under a visible-light source. The enhanced photocatalytic activity of CuS/Co_2SiO_4 -30 composite which degrades 88% of MB could be coming from the synergistic interaction effect of CuS and Co_2SiO_4, with a prolonged lifetime of photo-induced electron-hole pair. According to the PL result, the synergistic interaction between CuS and Co_2SiO_4, thereby improving the charge carrier separation and increasing the photocatalytic activity of the composite materials. The recyclability tests showed the stability of the synthesized composite materials up to 3rd cycles.

6. REFERENCES

1. Rosenwinkel, K.-H., U. Austermann-Haun, and H. Meyer, *Industrial wastewater sources and treatment strategies.* Environmental biotechnology: Concepts and applications, 2005.

2. Rasheed, T., et al., *Environmentally-related contaminants of high concern: Potential sources and analytical modalities for detection, quantification, and treatment.* Environment International, 2019. **122**: p. 52-66.

3. Cardenas, M.A.R., et al., *Removal of micropollutants through a biological wastewater treatment plant in a subtropical climate, Queensland-Australia.* Journal of Environmental Health Science and Engineering, 2016. **14**(1): p. 1-10.

4. Mustapha, S., et al., *Application of TiO_2 and ZnO nanoparticles immobilized on clay in wastewater treatment: a review.* Applied Water Science, 2020. **10**(1): p. 1-36.

5. Soltani, R.D.C., et al., *Ultrasonically induced ZnO–biosilica nanocomposite for degradation of a textile dye in aqueous phase.* Ultrasonics sonochemistry, 2016. **28**: p. 69-78.

6. Asghar, A., A.A. Abdul Raman, and W.M.A. Wan Daud, *Advanced oxidation processes for in-situ production of hydrogen peroxide/hydroxyl radical for textile wastewater treatment: a review.* Journal of Cleaner Production, 2015. **87**: p. 826-838.

7. El-Hout, S.I., et al., *Highly efficient sunlight-driven photocatalytic degradation of malachite green dye over reduced graphene oxide-supported CuS nanoparticles.* Journal of Alloys and Compounds, 2020. **849**: p. 156573.

8. Ayodhya, D. and G. Veerabhadram, *A review on recent advances in photodegradation of dyes using doped and heterojunction based semiconductor metal sulfide nanostructures for environmental protection.* Materials today energy, 2018. **9**: p. 83-113.

9. Pejjai, B., M. Reddivari, and T.R.R. Kotte, *Phase controllable synthesis of CuS nanoparticles by chemical co-precipitation method: Effect of copper precursors on the properties of CuS.* Materials Chemistry and Physics, 2020. **239**: p. 122030.

10. Saranya, M., et al., *Enhanced visible light photocatalytic reduction of organic pollutant and electrochemical properties of CuS catalyst.* Powder Technology, 2015. **279**: p. 209-220.

11. Ren, H., et al., *Synthesis and properties of nanoporous Ag_2S/CuS catalyst for hydrogen evolution reaction.* Electrochimica Acta, 2016. **190**: p. 221-228.

12. Liu, J. and D. Xue, *Rapid and scalable route to CuS biosensors: a microwave-assisted Cu-complex transformation into CuS nanotubes for ultrasensitive nonenzymatic glucose sensor.* Journal of Materials Chemistry, 2011. **21**(1): p. 223-228.

13. Zhang, X., et al., *CuS nanotubes for ultrasensitive nonenzymatic glucose sensors.* Chemical communications, 2008(45): p. 5945-5947.

14. Wang, Y., et al., *Ternary nanocomposites of Au/CuS/TiO_2 for an ultrasensitive photoelectrochemical non-enzymatic glucose sensor.* Analyst, 2018. **143**(7): p. 1699-1704.

15. Qian, L., et al., *In situ synthesis of CuS nanotubes on Cu electrode for sensitive nonenzymatic glucose sensor.* Sensors and Actuators B: Chemical, 2013. **176**: p. 952-959.

16. Gu, X., et al., *CuS nanoparticles as a photodynamic nanoswitch for abrogating bypass signaling to overcome gefitinib resistance.* Nano letters, 2019. **19**(5): p. 3344-3352.

17. Han, Y., et al., *Synthesis of novel CuS with hierarchical structures and its application in lithium-ion batteries.* Powder technology, 2011. **212**(1): p. 64-68.

18. Wang, Y., et al., *In situ preparation of CuS cathode with unique stability and high rate performance for lithium ion batteries.* Electrochimica acta, 2012. **80**: p. 264-268.

19. Wang, P., et al., *MOF-derived CuS@ Cu-BTC composites as high-performance anodes for lithium-ion batteries.* Small, 2019. **15**(47): p. 1903522.

20. AL-Jawad, S.M., A.A. Taha, and A.M. Redha, *Studying the structural, morphological, and optical properties of CuS: Ni nanostructure prepared by a hydrothermal method for biological activity*. Journal of Sol-Gel Science and Technology, 2019. **91**(2): p. 310-323.

21. Zhao, R., et al., *Polypyrrole-modified CuS nanoprisms for efficient near-infrared photothermal therapy.* RSC advances, 2017. **7**(17): p. 10143-10149.

22. Song, W., et al., *Application of a cation-exchange reaction of CuS nanoparticles and fluorescent copper nanoparticles in a DNA biosensor.* RSC advances, 2018. **8**(27): p. 15248-15252.

23. Feng, X., et al., *Controlled growth and field emission properties of CuS nanowalls.* Nanotechnology, 2007. **18**(14): p. 145706.

24. Geetha, D., et al., *Nanoporous transition metal sulfide (Cd–CuS) active electrode material for electrochemical energy storage device.* Journal of Materials Science: Materials in Electronics, 2020. **31**(2): p. 983-993.

25. Zeinodin, R., F. Jamali-Sheini, and M. Cheraghizade, *Physical properties of Pb-doped CuS nanostructures for optoelectronic applications.* Materials Science in Semiconductor Processing, 2021. **123**: p. 105501.

26. Guo, X., et al., *Photoelectrochromic smart windows powered by flexible dye-sensitized solar cell using CuS mesh as counter electrode.* Materials Letters, 2019. **244**: p. 92-95.

27. D'Souza, L.P., et al., *Neodymium doped titania as photoanode and graphene oxide-CuS composite as counter electrode material in quantum dot solar cell.* Journal of Materials Research, 2015. **30**(21): p. 3241.

28. Fu, Y. and W. Jin, *Facile synthesis of core-shell CuS-Cu_2S based nanocomposite for the high-performance glucose detection.* Materials Science and Engineering: C, 2019. **105**: p. 110120.

29. Kalanur, S.S., Y.-A. Lee, and H. Seo, *Eye-readable gasochromic and optical hydrogen gas sensor based on CuS–Pd.* RSC advances, 2015. **5**(12): p. 9028-9034.

30. Pathania, D., et al., *Fabrication of chitosan-g-poly (acrylamide)/CuS nanocomposite for controlled drug delivery and antibacterial activity.* Materials Science and Engineering: C, 2016. **64**: p. 428-435.

31. Tao, F., et al., *Structural evolution from CuS nanoflowers to Cu 9 S 5 nanosheets and their applications in environmental pollution removal and photothermal conversion.* RSC advances, 2016. **6**(68): p. 63820-63826.

32. Dhasade, S., et al., *Copper sulfide nanorods grown at room temperature for photovoltaic application.* Materials Letters, 2013. **90**: p. 138-141.

33. Cheng, Y., et al., *Coupled cobalt silicate nanobelt-on-nanobelt hierarchy structure with reduced graphene oxide for enhanced supercapacitive performance.* Journal of Power Sources, 2020. **448**: p. 227407.

34. Stoia, M., et al., *Low temperature synthesis of Co_2SiO_4/SiO_2 nanocomposite using a modified sol–gel method.* Journal of Sol-Gel Science and Technology, 2010. **54**(1): p. 49-56.

35. Kababji, A.H., B. Joseph, and J.T. Wolan, *Silica-Supported Cobalt Catalysts for Fischer–Tropsch Synthesis: Effects of Calcination Temperature and Support Surface Area on Cobalt Silicate Formation.* Catalysis Letters, 2009. **130**(1): p. 72-78.

36. Jabłoński, J.M., M. Wołcyrz, and L. Krajczyk, *On Cobalt Silicate Formation during High-Temperature Calcination of Impregnated Cobalt/Silica Catalysts.* Journal of Catalysis, 1998. **173**(2): p. 530-534.

37. Puskas, I., et al., *Novel aspects of the physical chemistry of Co/SiO2 Fischer–Tropsch catalyst preparations: The chemistry of cobalt silicate formation during catalyst preparation or hydrogenation.* Applied Catalysis A: General, 2006. **311**: p. 146-154.

38. Girardon, J.-S., et al., *Effect of cobalt precursor and pretreatment conditions on the structure and catalytic performance of cobalt silica-supported Fischer–Tropsch catalysts.* Journal of Catalysis, 2005. **230**(2): p. 339-352.

39. Cantalini, C., et al., *Gas sensing properties of nanocrystalline NiO and Co_3O_4 in porous silica sol–gel films.* Sensors and Actuators B: Chemical, 2005. **108**(1): p. 184-192.

40. Mueller, F., et al., *Cobalt orthosilicate as a new electrode material for secondary lithium-ion batteries.* Dalton Transactions, 2014. **43**(40): p. 15013-15021.

41. Dong, Q., et al., *Template-Free Synthesis of Cobalt Silicate Nanoparticles Decorated Nanosheets for High Performance Lithium Ion Batteries.* ACS Sustainable Chemistry & Engineering, 2018. **6**(11): p. 15591-15597.

42. Yang, J., et al., *Cobalt silicate hierarchical hollow spheres for lithium-ion batteries.* Nanotechnology, 2016. **27**(36): p. 365401.

43. Cheng, W., et al., *Amorphous cobalt silicate nanobelts@ carbon composites as a stable anode material for lithium ion batteries.* Chemical science, 2015. **6**(12): p. 6908-6915.

44. Wang, Q., et al., *Designed mesoporous hollow sphere architecture metal (Mn, Co, Ni) silicate: A potential electrode material for flexible all solid-state asymmetric supercapacitor.* Chemical Engineering Journal, 2019. **362**: p. 818-829.

45. Cheng, Y., et al., *Synthesis of amorphous cobalt silicate nanobelts@manganese silicate core–shell structures as enhanced electrode for high-performance hybrid supercapacitors.* Journal of Colloid and Interface Science, 2020. **561**: p. 762-771.

46. Cheng, Y., Y. Zhang, and C. Meng, *Template Fabrication of Amorphous Co_2SiO_4 Nanobelts/Graphene Oxide Composites with Enhanced Electrochemical Performances for Hybrid Supercapacitors.* ACS Applied Energy Materials, 2019. **2**(5): p. 3830-3839.

47. Bayat, S., D. Ghanbari, and M. Salavati-Niasari, *Pechini synthesis of Co_2SiO_4 magnetic nanoparticles and its application in photo-degradation of azo dyes.* Journal of Molecular Liquids, 2016. **220**: p. 223-231.

48. Shao, P., et al., *Cobalt silicate hydroxide nanosheets in hierarchical hollow architecture with maximized cobalt active site for catalytic oxidation.* Chemical Engineering Journal, 2019. **359**: p. 79-87.

49. Adepu, A., R. Anumula, and N. Venkatathri, *Synthesis and Characterization of Magnetically Separable Porous Titanium Silicate Nanocomposite Catalyst for Environmental Applications.* Materials today: proceedings, 2017. **4**: p. 19-24.

50. McGuinness, N., et al., *Nanotechnology Solutions for Global Water Challenges*. 2015. p. 375-411.

51. Feng, T., et al., *One-Dimensional Nanostructured TiO $_2$ for Photocatalytic Degradation of Organic Pollutants in Wastewater.* International Journal of Photoenergy, 2014. **2014**: p. 1-14.

52. Das, R., et al., *Sonocatalytic rapid degradation of Congo red dye from aqueous solution using magnetic Fe0/polyaniline nanofibers.* Ultrasonics sonochemistry, 2017. **37**: p. 600-613.

53. Chen, H., et al., *Kernel functions embedded in support vector machine learning models for rapid water pollution assessment via near-infrared spectroscopy.* Science of The Total Environment, 2020. **714**: p. 136765.

54. Balasuriya, A., *Chapter 25 - Coastal Area Management: Biodiversity and Ecological Sustainability in Sri Lankan Perspective*, in *Biodiversity and Climate Change Adaptation in Tropical Islands*, C. Sivaperuman, et al., Editors. 2018, Academic Press. p. 701-724.

55. Arenas-Sánchez, A., A. Rico, and M. Vighi, *Effects of water scarcity and chemical pollution in aquatic ecosystems: state of the art.* Science of the Total Environment, 2016. **572**: p. 390-403.

56. Xiao, L., J. Liu, and J. Ge, *Dynamic game in agriculture and industry cross-sectoral water pollution governance in developing countries.* Agricultural Water Management, 2021. **243**: p. 106417.

57. Anh, H.Q., et al., *Antibiotics in surface water of East and Southeast Asian countries: A focused review on contamination status, pollution sources, potential risks, and future perspectives.* Science of The Total Environment, 2020: p. 142865.

58. Nasrollahzadeh, M., et al., *Green-synthesized nanocatalysts and nanomaterials for water treatment: Current challenges and future perspectives.* Journal of Hazardous Materials, 2020: p. 123401.

59. Holkar, C.R., et al., *A critical review on textile wastewater treatments: Possible approaches.* J Environ Manage, 2016. **182**: p. 351-366.

60. Pandey, A., P. Singh, and L. Iyengar, *Bacterial decolorization and degradation of azo dyes.* International Biodeterioration & Biodegradation, 2007. **59**(2): p. 73-84.

61. Kaykhaii, M., M. Sasani, and S. Marghzari, *Removal of Dyes from the Environment by Adsorption Process.* Chemical and Materials Engineering, 2018. **6**(2): p. 31-35.

62. Katheresan, V., J. Kansedo, and S.Y. Lau, *Efficiency of various recent wastewater dye removal methods: a review.* Journal of environmental chemical engineering, 2018. **6**(4): p. 4676-4697.

63. Fujishima, A. and K. Honda, *Electrochemical photolysis of water at a semiconductor electrode.* nature, 1972. **238**(5358): p. 37-38.

64. Koe, W.S., et al., *An overview of photocatalytic degradation: photocatalysts, mechanisms, and development of photocatalytic membrane.* Environmental Science and Pollution Research, 2020. **27**(3): p. 2522-2565.

65. Anwer, H., et al., *Photocatalysts for degradation of dyes in industrial effluents: opportunities and challenges.* Nano Research, 2019. **12**(5): p. 955-972.

66. El-Salamony, R.A., et al., *Visible light sensitive activated carbon-metal oxide (TiO_2, WO3, NiO, and SnO) nano-catalysts for photo-degradation of methylene blue: a comparative study.* Toxicological & Environmental Chemistry, 2018. **100**(2): p. 143-156.

67. Hernández-Ramírez, A. and I. Medina-Ramírez, *Photocatalytic semiconductors*. 2016: Springer.

68. Ren, H., et al., *Photocatalytic materials and technologies for air purification.* Journal of hazardous materials, 2017. **325**: p. 340-366.

69. Chai, Z., et al., *Synthesis of 3D hierarchical CuS architectures consisting of 1D nanotubes for efficient photocatalysts.* Materials Letters, 2020. **275**: p. 128168.

70. Yoo, J.-H., et al., *Facile synthesis of hierarchical CuS microspheres with high visible-light-driven photocatalytic activity.* Journal of Photochemistry and Photobiology A: Chemistry, 2020. **401**: p. 112782.

71. Wang, W. and L. Ao, *Synthesis and characterization of crystalline CuS nanorods prepared via a room temperature one-step, solid-state route.* Materials Chemistry and Physics, 2008. **109**(1): p. 77-81.

72. Ji, H., et al., *Fabrication of CuS nanocrystals with various morphologies in the presence of a nonionic surfactant.* Materials Letters, 2005. **59**(24-25): p. 3169-3172.

73. Saranya, M., et al., *Growth of CuS Nanostructures by Hydrothermal Route and Its Optical Properties.* Journal of Nanotechnology, 2014. **2014**: p. 321571.

74. Ghanbari, D., et al., *Hydrothermal synthesis of CuS nanostructures and their application on preparation of ABS-based nanocomposite.* Journal of Industrial and Engineering Chemistry, 2014. **20**(5): p. 3709-3713.

75. Saranya, M. and d.A. Nirmala Grace. *Hydrothermal synthesis of CuS nanostructures with different morphology*. in *Journal of Nano Research*. 2012. Trans Tech Publ.

76. Hosseinpour, Z., et al., *A controlled solvothermal synthesis of CuS hierarchical structures and their natural-light-induced photocatalytic properties.* New Journal of Chemistry, 2015. **39**(7): p. 5470-5476.

77. Liu, J. and D. Xue, *Solvothermal synthesis of CuS semiconductor hollow spheres based on a bubble template route.* Journal of crystal growth, 2009. **311**(3): p. 500-503.

78. Zhang, Y.Q., et al., *Preparation by solvothermal synthesis, growth mechanism, and photocatalytic performance of CuS nanopowders.* European Journal of Inorganic Chemistry, 2014. **2014**(14): p. 2368-2375.

79. Larsen, T.H., et al., *Solventless synthesis of copper sulfide nanorods by thermolysis of a single source thiolate-derived precursor.* Journal of the American Chemical Society, 2003. **125**(19): p. 5638-5639.

80. Xu, H., W. Wang, and W. Zhu, *Sonochemical synthesis of crystalline CuS nanoplates via an in situ template route.* Materials Letters, 2006. **60**(17-18): p. 2203-2206.

81. Xiao, S., et al., *General and facile synthesis of metal sulfide nanostructures: In situ microwave synthesis and application as binder-free cathode for Li-ion batteries.* Chemical Engineering Journal, 2016. **306**: p. 251-259.

82. Wan, S., et al., *Single-step synthesis of copper sulfide hollow spheres by a template interface reaction route.* Journal of Materials Chemistry, 2004. **14**(16): p. 2489-2491.

83. Nagarathinam, M., J. Chen, and J.J. Vittal, *From self-assembled Cu (II) coordination polymer to shape-controlled CuS nanocrystals.* Crystal Growth and Design, 2009. **9**(5): p. 2457-2463.

84. Dhasade, S., et al., *Synthesis of CuS nanorods grown at room temperature by electrodeposition method.* Materials Chemistry and Physics, 2012. **137**(1): p. 353-358.

85. Saranya, M., et al., *Hydrothermal growth of CuS nanostructures and its photocatalytic properties.* Powder technology, 2014. **252**: p. 25-32.

86. Goble, R., *COPPER SULFIDES FROM ALBERTA: YARROWITE GusSs AND SPIONKOPITE GuuoS, o.* Canadian Mineralogist, 1980. **18**: p. 511-518.

87. Hussain, S., et al., *Thermoelectric properties of Ag-doped CuS nanocomposites synthesized by a facile polyol method.* Physical Chemistry Chemical Physics, 2018. **20**(8): p. 5926-5935.

88. Casaca, A., et al., *Electrical transport properties of CuS single crystals.* Journal of Physics: Condensed Matter, 2011. **24**(1): p. 015701.

89. Morales-Garcia, A., et al., *First-Principles Calculations and Electron Density Topological Analysis of Covellite (CuS).* The journal of physical chemistry. A, 2014. **118**.

90. Tagirov, B., et al., *Covellite CuS*. 2016.

91. Tailor, J.P., *CuS single crystals thin films nanoparticles and their application.* 2014.

92. Casaca, A., et al., *Electrical transport properties of CuS single crystals.* Journal of Physics: Condensed Matter, 2011. **24**(1): p. 015701.

93. Chaki, S.H., J.P. Tailor, and M.P. Deshpande, *Covellite CuS – Single crystal growth by chemical vapour transport (CVT) technique and characterization.* Materials Science in Semiconductor Processing, 2014. **27**: p. 577-585.

94. Li, F., et al., *Controllable synthesis, optical and photocatalytic properties of CuS nanomaterials with hierarchical structures.* Powder Technology, 2010. **198**(2): p. 267-274.

95. Pavithra, K.G. and V. Jaikumar, *Removal of colorants from wastewater: a review on sources and treatment strategies.* Journal of Industrial and Engineering Chemistry, 2019. **75**: p. 1-19.

96. Natarajan, S., H.C. Bajaj, and R.J. Tayade, *Recent advances based on the synergetic effect of adsorption for removal of dyes from waste water using photocatalytic process.* Journal of Environmental Sciences, 2018. **65**: p. 201-222.

97. Pingmuang, K., et al., *Composite photocatalysts containing BiVO 4 for degradation of cationic dyes.* Scientific reports, 2017. **7**(1): p. 1-11.

98. Pal, M., et al., *Synthesis of CuS nanoparticles by a wet chemical route and their photocatalytic activity.* Journal of Nanoparticle Research, 2015. **17**(7): p. 1-12.

99. Al-Mamun, M., et al., *Photocatalytic activity improvement and application of UV-TiO_2 photocatalysis in textile wastewater treatment: A review.* Journal of Environmental Chemical Engineering, 2019. **7**(5): p. 103248.

100. Katagi, T., *Direct photolysis mechanism of pesticides in water*. Journal of pesticide science, 2018. **43**(2): p. 57-72.

101. Isac, L., et al., *Copper sulfide based heterojunctions as photocatalysts for dyes photodegradation.* Frontiers in chemistry, 2019. **7**: p. 694.

102. Huang, Y., et al., *Catalytic degradation of ciprofloxacin by magnetic $CuS/Fe_2O_3/Mn_2O_3$ nanocomposite activated peroxymonosulfate: Influence factors, degradation pathways and reaction mechanism.* Chemical Engineering Journal, 2020. **388**: p. 124274.

103. Chen, J., et al., *Synthesis of flower-like CuS/UiO-66 composites with enhanced visible-light photocatalytic performance.* Inorganic Chemistry Communications, 2019. **104**: p. 223-228.

104. Sreelekha, N., et al., *Structural, optical, magnetic and photocatalytic properties of Co doped CuS diluted magnetic semiconductor nanoparticles.* Applied Surface Science, 2016. **378**: p. 330-340.

105. Sreelekha, N., et al., *Efficient photocatalytic degradation of rhodamine-B by Fe doped CuS diluted magnetic semiconductor nanoparticles under the simulated sunlight irradiation.* Solid State Sciences, 2016. **62**: p. 71-81.

106. Subramanyam, K., et al., *Chemical synthesis, structural, optical, magnetic characteristics and enhanced visible light active photocatalysis of Ni doped CuS nanoparticles.* Solid State Sciences, 2017. **65**: p. 68-78.

107. Hosseinpour, Z. and S. Hosseinpour, *Facile synthesis of Er: CuS flowers and their application in the photo-catalytic activity.* Materials Science in Semiconductor Processing, 2017. **72**: p. 32-36.

108. Zeinodin, R. and F. Jamali-Sheini, *In-doped CuS nanostructures: Ultrasonic synthesis, physical properties, and enhanced photocatalytic behavior.* Physica B: Condensed Matter, 2019. **570**: p. 148-156.

109. Ren, Y., D. Zeng, and W.-J. Ong, *Interfacial engineering of graphitic carbon nitride (g-C3N4)-based metal sulfide heterojunction photocatalysts for energy conversion: a review.* Chinese Journal of Catalysis, 2019. **40**(3): p. 289-319.

110. Basu, M., N. Garg, and A.K. Ganguli, *A type-II semiconductor (ZnO/CuS heterostructure) for visible light photocatalysis.* Journal of Materials Chemistry A, 2014. **2**(20): p. 7517-7525.

111. Meng, N., et al., *CuS/MoS $_2$ nanocomposite with high solar photocatalytic activity.* Journal of Nanoparticle Research, 2015. **17**(7): p. 1-10.

112. Mahanthappa, M., N. Kottam, and S. Yellappa, *Enhanced photocatalytic degradation of methylene blue dye using CuSCdS nanocomposite under visible light irradiation.* Applied Surface Science, 2019. **475**: p. 828-838.

113. Wu, C., et al., *Fabrication of CuS/CuO nanowire heterostructures on copper mesh with improved visible light photocatalytic properties.* Journal of Physics and Chemistry of Solids, 2020. **140**: p. 109355.

114. Wang, Y., et al., *Depositing of CuS nanocrystals upon the graphene scaffold and their photocatalytic activities.* Applied surface science, 2014. **303**: p. 54-60.

115. Hu, X.-S., et al., *Preparation of flower-like CuS/reduced graphene oxide (RGO) photocatalysts for enhanced photocatalytic activity.* Journal of Physics and Chemistry of Solids, 2017. **103**: p. 201-208.

116. ChongYeon, P., et al., *Preparation of CuS-graphene oxide/TiO_2 composites designed for high photonic effect and photocatalytic activity under visible light.* Chinese Journal of Catalysis, 2013. **34**(4): p. 711-717.

117. Bano, Z., et al., *Mesoporous CuS nanospheres decorated rGO aerogel for high photocatalytic activity towards Cr (VI) and organic pollutants.* Chemosphere, 2020. **246**: p. 125846.

118. Chen, X., et al., *Facile fabrication of novel porous graphitic carbon nitride/copper sulfide nanocomposites with enhanced visible light driven photocatalytic performance.* Journal of colloid and interface science, 2016. **476**: p. 132-143.

119. Wang, Q., et al., *Fabrication of the carnation-like CCN-CuS p–n heterojunctions with enhanced photocatalytic performance under visible light irradiation.* Applied Surface Science, 2016. **367**: p. 109-117.

120. Bai, Y., et al., *Synthesis of novel ternary heterojunctions via Bi_2WO_6 coupling with CuS and g-C_3N_4 for the highly efficient visible-light photodegradation of ciprofloxacin*

in wastewater. Colloids and Surfaces A: Physicochemical and Engineering Aspects, 2021. **610**: p. 125481.

121. Dutta, V., et al., *Fabrication of visible light active $BiFeO_3$/CuS/SiO2 Z-scheme photocatalyst for efficient dye degradation.* Materials Letters, 2020. **270**: p. 127693.

122. Guo, H., et al., *Facile fabrication of ZnO/CuS heterostructure photoanode with highly PEC performance and excellent charge separation efficiency.* Journal of Electroanalytical Chemistry, 2019. **854**: p. 113546.

123. Chen, Q., et al., *Construction of immobilized 0D/1D heterostructure photocatalyst Au/CuS/CdS/TiO_2 NBs with enhanced photocatalytic activity towards moxifloxacin degradation.* Chemical Engineering Journal, 2020. **389**: p. 124476.

124. Wang, X., et al., *Carbon quantum dots decorated CuS nanocomposite for effective degradation of methylene blue and antibacterial performance.* Journal of Molecular Liquids, 2018. **268**: p. 578-586.

125. Bai, Y., et al., *Synthesis of Novel Ternary Heterojunctions via Bi_2WO_6 coupling with CuS and g-C_3N_4 for the Highly Efficient Visible-light Photodegradation of Ciprofloxacin in Wastewater.* Colloids and Surfaces A: Physicochemical and Engineering Aspects, 2020: p. 125481.

126. YATABE, J., et al., *Synthesis of cobalt silicate using water glass as raw materials.* Journal of the Ceramic Society of Japan, 1997. **105**(1218): p. 188-191.

127. Bayat, S., A. Sobhani, and M. Salavati-Niasari, *Co_2SiO_4 nanostructures: New simple synthesis, characterization and investigation of optical property.* Materials Research Bulletin, 2017. **88**: p. 248-257.

128. Lan, D., et al., *Double-shell hollow glass microspheres@Co_2SiO_4 for lightweight and efficient electromagnetic wave absorption.* Chemical Engineering Journal, 2021. **408**: p. 127313.

129. Ali, A.A. and I.S. Ahmed, *Sol-gel auto-combustion fabrication and optical properties of cobalt orthosilicate: Utilization as coloring agent in polymer and ceramic.* Materials Chemistry and Physics, 2019. **238**: p. 121888.

130. Sun, Q., et al., *A cobalt silicate modified $BiVO_4$ photoanode for efficient solar water oxidation.* Applied Catalysis B: Environmental, 2020. **277**: p. 119189.

131. Hao, S.-M., et al., *Hierarchical mesoporous cobalt silicate architectures as high-performance sulfate-radical-based advanced oxidization catalysts.* Journal of Colloid and Interface Science, 2019. **545**: p. 128-137.

132. Christy, A.A., O.M. Kvalheim, and R.A. Velapoldi, *Quantitative analysis in diffuse reflectance spectrometry: a modified Kubelka-Munk equation.* Vibrational Spectroscopy, 1995. **9**(1): p. 19-27.

133. dzimbeg-malcic, V., Z. Barbaric-Mikocevic, and K. Itrić, *Kubelka-Munk theory in describing optical properties of paper (I).* Tehnicki Vjesnik, 2012. **19**: p. 191-196.

134. Holzwarth, U. and N. Gibson, *The Scherrer equation versus the'Debye-Scherrer equation'.* Nature nanotechnology, 2011. **6**(9): p. 534-534.

135. Hemalatha, K., et al., *Synthesis, characterization and optical properties of hybrid PVA–ZnO nanocomposite: a composition dependent study.* Materials Research Bulletin, 2014. **51**: p. 438-446.

136. Ayodhya, D. and G. Veerabhadram, *Facile fabrication, characterization and efficient photocatalytic activity of surfactant free ZnS, CdS and CuS nanoparticles.* Journal of Science: Advanced Materials and Devices, 2019. **4**(3): p. 381-391.

137. Ramamoorthy, C. and V. Rajendran, *Synthesis and characterization of CuS nanostructures: Structural, optical, electrochemical and photocatalytic activity by the hydro/solvothermal process.* International Journal of Hydrogen Energy, 2017. **42**(42): p. 26454-26463.

138. Kim, J.S., et al., *Amorphous cobalt phyllosilicate with layered crystalline motifs as water oxidation catalyst.* Advanced Materials, 2017. **29**(21): p. 1606893.

139. Biswas, S., et al., *Template-Free Synthesis of "Wool-Ball"-Like Hollow CuS Structures Can Effectively Suppress Electromagnetic Radiation: A Mechanistic Insight.* The Journal of Physical Chemistry C, 2019. **123**(28): p. 17136-17147.